DP - 505

Reactors - Power

AEC Research and Development Report

HEAVY WATER MODERATED POWER REACTORS

PROGRESS REPORT

May 1960

Technical Division

Wilmington, Delaware

July 1960

E. I. du Pont de Nemours & Co.
Explosives Department - Atomic Energy Division
Technical Division - Wilmington, Delaware

Printed in USA. Price $1.75
Available from the Office of Technical Services
U. S. Department of Commerce
Washington 25, D. C.

✓ 255422

DP - 505

2ND ISSUE

REACTORS - POWER
(TID-4500, 15th Ed.)

HEAVY WATER MODERATED POWER REACTORS

Progress Report
May 1960

D. F. Babcock, Coordinator
Power Reactor Studies
Wilmington, Delaware

Compiled by R. R. Hood and L. Isakoff

July 1960

E. I. du Pont de Nemours & Co.
Explosives Department - Atomic Energy Division
Technical Division - Wilmington, Delaware

Printed by Savannah River Laboratory for
The United States Atomic Energy Commission
Contract AT(07-2)-1

ABSTRACT

A Zircaloy-clad tube of unalloyed uranium that was irradiated in a loop of the NRU reactor to a maximum exposure of 950 MWD/T at a maximum uranium temperature of 400°C experienced less than 1.5% volume increase and 0.14% outer cladding strain. Inspection of the swaged oxide tube that had failed during irradiation in a Savannah River reactor revealed that a 9-inch-long crack of as-yet-unknown origin had developed in the outer stainless steel cladding of the tube. Transient calculations showed that boiling D_2O reactors that are fueled with uranium metal probably would not operate stably as presently designed, but that those fueled with uranium oxide operating at high fuel temperature probably would be stable. A computer code for the calculation of the lattice bucklings of D_2O-moderated reactors is described. A description is presented of the tandem extrusion process that was developed by Nuclear Metals, Inc., for the fabrication of bonded joints of Zircaloy and stainless steel.

CONTENTS

LIST OF TABLES AND FIGURES

HEAVY WATER MODERATED POWER REACTORS

Progress Report
May 1960

INTRODUCTION

This report is one of a series that records the progress of the du Pont study of power reactors that are moderated by heavy water and fueled with natural uranium. The present effort is divided into two main categories: (1) the development required for the successful design, construction, and operation of the Heavy Water Components Test Reactor (HWCTR), a facility for irradiating fuel elements at power reactor conditions, and (2) the development of the technology of full-scale D_2O-moderated power reactors. Earlier reports in the series are:

DP-232	DP-375	DP-445
DP-245	DP-385	DP-455
DP-265	DP-395	DP-465
DP-285	DP-405	DP-475
DP-295	DP-415	DP-485
DP-315	DP-425	DP-495
DP-345	DP-435	

Progress during June 1960 will be reported in DP-515.

SUMMARY

The Zircaloy-clad tube of unalloyed uranium that is being irradiated in the NRU reactor was examined after reaching a maximum exposure of 950 MWD/T at a maximum uranium temperature of 400°C. The results of the examination were generally satisfactory in that the maximum volume increase was less than 1.5% and the maximum strain in the outer cladding was only 0.14%. Mechanical difficulties precluded immediate reinsertion of the tube into the reactor.

Inspection of the assembly of swaged oxide tubes that failed during irradiation in a Savannah River reactor revealed that the failure was in the outer sheath (stainless steel) of the central tube in the column. A 9-inch-long crack was visible in the cladding of this tube. Although several possible mechanisms have been postulated, the cause of the failure is not yet known.

Transient calculations for a design of a boiling D_2O reactor fueled with uranium metal indicate that this reactor probably would not be stable as presently designed because of positive void coefficients. It is doubtful that this problem can be overcome by any simple changes in the reactor parameters or in fuel element design. Although these findings are subject to confirmation by measurements of void and temperature coefficients, it appears that metal elements will not be suitable for boiling D_2O reactors. Oxide-fueled boiling reactors that

operate at high fuel temperature would be expected to operate stably because the negative temperature coefficient of the fuel should be high enough to override the positive void coefficient.

A computer code has been written for IBM 650 calculations of lattice bucklings of D_2O-moderated reactors. The code is based on the calculation methods that were described by the Savannah River Laboratory at the 1958 Geneva Conference. At present, the code is restricted to tubular fuel assemblies, but it will be extended to include clusters of rods and parallel plates.

A description is presented of the tandem extrusion process that was developed at Nuclear Metals for fabrication of bonded joints of Zircaloy and stainless steel. The various out-of-pile tests that have been performed on bonded joints are reviewed.

DISCUSSION

I. HEAVY WATER COMPONENTS TEST REACTOR (HWCTR)

The HWCTR is a test reactor that is being built at the Savannah River Plant primarily for irradiation tests of fuel elements at conditions that are representative of D_2O-moderated power reactors. The reactor is scheduled to be placed in operation in mid-1961. A description of the facility was presented in DP-383[1] and in earlier progress reports. Progress during May on design, construction, and supporting studies is reported in this section.

A. REACTOR STATUS

At the end of May, construction of the HWCTR was approximately 35% complete. Erection of the steelwork for the shell of the reactor building was started. Segments of the "T-flange" were welded together, and the welds were heat treated and inspected. This flange is bolted to the concrete substructure to form the main joint between the concrete and steel parts of the containment shell. Welding of the steel plates above the flange section is in progress.

B. STATUS OF ISOLATED COOLANT LOOPS

The mockup of the boiling loop bayonet and its discharge piping was completed (except for heat exchangers) and hydrostatically tested. A description of the mockup, which is to be used for vibration studies and flow tests, was presented in DP-485. Vibration tests are scheduled to begin in June.

An order has been placed with the Canadian Westinghouse Co. for a prototype of the 5-inch joints to be provided between Zircaloy and stainless steel in the two reactor bayonets. The quality of this joint will be assessed by subjecting the prototype to thermal and pressure cycles. The design is that of a so-called "graded" joint in which the difference in coefficients of thermal expansion of Zircaloy and stainless steel is taken up gradually by interposing a series of rings of nickel-iron alloys with progressively different coefficients of expansion. A similar joint is presently in service in the E-20 loop of the NRU reactor. The design of the prototype is shown in Figure 1. As shown in this figure, the seal is by means of a conical gasket of gold that is loaded mechanically as the two nickel-iron pieces are welded together. Shrinkage of the latter pieces after welding further loads the gasket. The principal differences between the prototype and the bayonet joints are that in the former the Zircaloy part is a cap instead of a tube and the 43% nickel - 57% iron section is welded directly to carbon steel pipe rather than to another ring of lower nickel content.

C. SAFEGUARDS ANALYSIS OF BOILING LOOP

Calculations were made of the transient response of cooling conditions in the boiling D_2O loop of the HWCTR to (1) changes in the distribution of D_2O flow through the loop, and (2) accidental reactivity additions. The results of the calculations indicate the conditions under which these situations will lead to incomplete quenching of the steam that is generated in the loop and, eventually, to loss of coolant for the fuel assembly.

The results of earlier calculations of transients in the boiling loop were reviewed in DP-485, which also included a description of the mathematical model of the loop and the calculation procedures. Initial conditions for all of the transients reported thus far are as follows:

Reactor power - 30 MW

Loop pressure (equals reactor pressure) - 795 psia

Inlet temperature of cooling water to loop heat exchanger - 22°C

It is assumed unless otherwise stated that the coolant flow through the fuel assembly in the loop remains constant. The direct effects of the transients on the burnout safety factor in the fuel assembly have not been considered yet.

1. Effect of Bypassing the Fuel Assembly

When the flow of D_2O through the fuel assembly is decreased, the steam quality of the effluent from the assembly increases. Figure 2 shows the steam quality as a function of the fraction, f_1, of total loop D_2O flow that passes through the test assembly when a constant f_3 (0.4) of the total flow is passed through the heat exchanger that is in parallel with the test assembly. If the flow through the test assembly is decreased at constant f_3, the fraction f_2 that bypasses both the test assembly and the heat exchanger must be increased correspondingly. Under these conditions, both the steam quality and the D_2O temperature at the inlet to the steam quencher increase. Figure 3 shows the rates of increase for three linear rates of increase in the bypass flow.

2. Effect of Bypassing the Heat Exchanger

If the rate of D_2O flow through the heat exchanger is reduced while the power generation and D_2O flow in the test assembly are held constant, the D_2O temperatures at the inlet and outlet of the steam quencher increase. In turn, the subcooling of the inlet D_2O to the test assembly decreases and the exit steam quality increases. Figure 4 shows the transients that follow a linear reduction of f_3 from 0.4 to 0.3 in 5 seconds. With f_1 constant at 0.6, f_2 must rise from zero to 0.1. In this case, the temperature of the D_2O at the quencher outlet rises

almost to the saturation temperature. If f_3 were reduced to 0.28, the D_2O would leave the quencher at the saturation temperature; a further reduction of f_3 would result in a mixture of D_2O liquid and D_2O steam emerging from the quencher.

3. Effect of Ramp Addition of Reactivity

If two control rods are driven out of the HWCTR at maximum speed as the result of operator error or failure of the gang control switch, reactivity is added at a rate of 0.0003 k/sec. This accident is self-limiting as far as the reactor itself is concerned, even if the scram circuits fail to function (see DP-383)[1]. It is seen from Figure 5 that in the boiling loop the steam quality at the outlet of the fuel assembly rises rapidly. Within 5 seconds the temperature of the D_2O at the quencher outlet increases to the saturation temperature. If the reactor is not scrammed, D_2O steam will flow into the reactor and the test assembly will be deprived of coolant.

4. Effect of Step Addition of Reactivity

If a half rod falls from the midplane of the reactor to the bottom as a result of a broken latch, the reactivity is suddenly increased by as much as 0.006 k. For a reactivity increase of this magnitude, there is insufficient time for the safety rods to prevent coolant boiling and local fuel melting in the reactor (see DP-383).[1] For reactivity increases of less than 0.004 k, the accident is self-limiting as far as the reactor itself is concerned. In the boiling loop, a step increase in reactivity of 0.004 k causes the D_2O temperature at the steam quencher outlet to reach the saturation temperature in less than 0.5 second, after which D_2O steam will begin to flow into the reactor vessel. Figure 6 shows that the loop can tolerate a step reactivity increase of 0.001 k, although the margin between the steam quencher outlet temperature and the saturation temperature is only 3°C at one point (6 seconds after the Δk introduction).

D. FLOW TESTS

A flow test of a mockup of a fuel assembly for irradiation of rods of uranium oxide in the HWCTR was started in deionized water at 260°C. The design of the fuel assembly was previously described in DP-485 and DP-495. The mockup contains a bundle of 19 rods of stainless steel tubing, 0.540 inch in OD, that are filled with lead to simulate the weight of the oxide rods. The test bundle, which is 3.10 inches in OD, is assembled in a stainless steel housing tube of 3.18 inches in ID. The resulting diametral clearance of 0.080 inch is about twice the design clearance of 0.038 inch. Deionized water is supplied to the test assembly at a flow of about 260 gpm.

II. TECHNOLOGY OF FULL-SCALE REACTORS

A. PHYSICS

1. Stability of Boiling-D_2O-Cooled Reactors

Studies of the stability of boiling-D_2O-cooled power reactors operating on a direct steam cycle indicate that if such reactors were fueled with natural uranium metal, they probably would not operate in a stable manner. Oxide-fueled reactors of this type, however, are expected to operate stably. The calculations that led to these conclusions were carried out in two ways: (a) by analysis of the transfer functions associated with a greatly simplified representation of the system, and (b) by numerical integration of a set of equations that describe the system in more detail.

In order to obtain a sufficient amount of heat transfer surface for an economical boiling reactor, it is necessary to use fuel assemblies with a large internal surface. These assemblies might be clusters of thin concentric tubes or of many thin fuel rods. In such assemblies, the void coefficient is generally positive. If the fuel were uranium oxide and were to operate at a very high temperature, the negative temperature coefficient from the Doppler broadening of the U^{238} resonances might be sufficient to override the positive void coefficent and give the assembly a net negative power coefficient. In metal assemblies, on the other hand, the change in fuel temperature per fractional change of power is much smaller while the void coefficient itself is usually somewhat larger than for oxide assemblies. Thus, in metal fuel assemblies the net prompt power coefficient is likely to be positive.

The present study was directed toward determining ranges of values of the power coefficients for which such a system is stable or at least operable. The stabilities of both the power level and the power distribution in a large reactor were investigated. Further studies of boiling-D_2O-reactor stability are scheduled to include the experimental determination of the void coefficients of reactivity, so that a more accurate appraisal of the system can be made.

The discussion below is concerned primarily with metal-fueled reactors, but the methods described are equally applicable to the oxide-fueled reactors.

a. Transient Response by Transfer Function Analysis

A study was made by transfer function analysis of the ranges of values of the temperature and void coefficients for which a boiling D_2O reactor would be stable. The regions of stability were first determined by an analysis of the transfer functions for a greatly simplified representation of the reactor system. Particular points were then checked by numerical integration of the equations that describe the

reactor in more complete detail. The transfer function analysis was used to determine the regions for stability for both the power level and the power distribution within the reactor core.

The simplified representation of the boiling reactor system that was used in the transfer function analysis is shown in Figure 7. The heavy water coolant enters the fuel assemblies at an ambient temperature that is considered constant in time. The coolant boils inside the fuel channels and the steam-liquid mixture passes into a steam drum from which the steam flows into the turbine. In the reactor, the fuel assembly consists of fuel, coolant, and voids and is characterized by a temperature, T_f, and a power coefficient, α_f, that has a characteristic time constant, λ_f. The moderator is cooled by a separate cooling system and could be characterized by a moderator temperature, T_m, a power coefficient, α_m, and a characteristic time, λ_m. However, for the present calculations the moderator coefficient is considered to be too slowly acting to be of concern and is ignored. The steam drum is at a pressure, p. A fractional increase in the pressure results in a change of reactivity in the reactor through the pressure coefficient of reactivity, α_p, which acts with a characteristic time, λ_p.

For the analysis it was assumed that the prompt neutron lifetime is zero and that there is only a single group of delayed neutrons. The reactor kinetic equations are listed as Equations (1).

$$0 = M^2\nabla^2\phi + (k - 1)\phi - k\beta(\phi - C)$$

$$\frac{dC}{dt} = \lambda(\phi - C)$$

$$\frac{dT_f}{dt} = \lambda_f(\phi - T_f) \qquad (1)$$

$$\frac{dp}{dt} = \lambda_p(\phi - \phi_o)$$

$$k = k_o + \alpha_f(T_f - T_{fo}) - \alpha_p(p - p_o)$$

In Equations (1) the migration area, M^2, the time constants, λ_f and λ_p, and the power coefficients, α_f and α_p, are assumed to be constant in both space and time. The flux, ϕ, the multiplication constant, k, the concentration of delayed neutron precursors, C, the normalized fuel temperature, T_f, and the pressure, p, vary in both space and time. The subscripts, o, refer to initial steady-state conditions. The power coefficient associated with the fuel assembly is made up of two terms: one corresponding to the temperature coefficient of the fuel and one corresponding to the change in void fraction, ϵ, associated with a change in reactor power level at constant reactor pressure, or

$$\alpha_f = \left(\frac{\partial k}{\partial \phi}\right)_p = \frac{\partial k}{\partial T_f}\frac{\partial T_f}{\partial \phi} + \frac{\partial k}{\partial \epsilon}\left(\frac{\partial \epsilon}{\partial \phi}\right)_p \qquad (2)$$

Its time constant is given by

$$\lambda_f = \frac{P_o}{H_f(T_{fo} - T_{fa})} \qquad (3)$$

Where P_o is the power generated in the fuel in MW, H_f is the heat capacity of the fuel in MW-sec/^oC, and T_{fo} and T_{fa} are the temperatures of the fuel and of the ambient coolant, respectively, in ^oC.

The reactivity coefficient of the system pressure is given by

$$\alpha_p = \left(\frac{\partial k}{\partial p}\right)_\phi = \frac{\partial k}{\partial \epsilon}\left(\frac{\partial \epsilon}{\partial p}\right)_\phi \qquad (4)$$

and its time constant is given by

$$\lambda_p = \frac{P_o}{V_{so}} \qquad (5)$$

where P_o is the reactor power in MW and V_{so} is a measure of the volume of the steam drum in MW-sec of steam.

To obtain approximate solutions to Equations (1), the following mathematical steps were taken:

1. The equations were made linear by the assumption of small perturbations about the steady-state operating conditions and the subtraction of the steady-state conditions.

2. The time derivatives were eliminated by the taking of Laplace transforms of the equations. The transforms of the variables C, T_f, p, and k were eliminated from the resulting set of algebraic equations.

3. The spatial derivatives were eliminated by the expansion of the flux in terms of a set of eigenfunctions that is orthogonal to the unperturbed power distribution and satisfies the same boundary conditions as the reactor flux.

4. The spatial dependence was removed by successive multiplication by each of the orthogonal eigenfunctions and integration over the reactor volume.

The result of these steps is an infinite set of algebraic equations in the expansion coefficients that are the Laplace transforms of the amplitudes of the various spatial modes of the power distribution. If the expansion for the flux is cut off at a finite number of eigenfunctions the equations can be solved for the expansion coefficients.

However, the solution of these equations is greatly simplified if it is assumed that the coupling between the spatial modes of the power distribution is negligible. This coupling is through terms of the form ϕ or k weighted by the product of two orthogonal functions and integrated over the reactor volume. These terms are identically zero if the flux and reactivity are constant over the reactor volume.

If the coupling between modes is neglected, separate equations result for each of the expansion coefficients, the first two of which are as follows:

$$\left[- \bar{k}_o \sum \frac{\beta_i s}{s + \lambda_i} + \bar{\phi}_o \sum \frac{\alpha_j \lambda_j}{s + \lambda_j} + \frac{\alpha_p \lambda_p}{s} \right] A_o = 0$$

$$\left[- \mu_1^2 M^2 - \bar{k}_1 \sum \frac{\beta_i s}{s + \lambda_i} + \bar{\phi}_1 \sum \frac{\alpha_j \lambda_j}{s + \lambda_j} \right] A_1 = 0 \qquad (6)$$

In Equations (6), $\bar{k}_o$ and $\bar{\phi}_o$ are k and ϕ averaged over the reactor volume as weighted by the square of the unperturbed flux distribution. The quantities $\bar{k}_1$ and $\bar{\phi}_1$ are the averaged values of k and ϕ weighted by the square of the first harmonic of the flux distribution. The quantity μ_1^2 is the difference in buckling between that of the first harmonic of the flux distribution and that of the unperturbed flux distribution. The symbol β is the delayed neutron fraction.

In order for nontrivial solutions for perturbations in the power level or in the power distribution to exist, the terms in brackets in Equations (6) must each be equal to zero. The numerator of each term is a polynomial in the Laplace transform variable, s. The roots of these polynomials define a set of values, s_n, that describe the possible time behavior of small perturbations in the power level or in the first harmonic of the power distribution since such perturbations will behave as e^{snt}. If one of the s_n's has a positive real part, the system is unstable. The limits of stability correspond to those values of the reactor parameters for which one of the roots has a real part that is equal to zero.

If the approximation is made that $\bar{k}_o$, $\bar{\phi}_o$, $\bar{k}_1$, and $\bar{\phi}_1$ are all unity, the polynomials corresponding to the numerators of Equations (6) are as follows:

Power level

$$s^3 + a_2 s^2 + a_1 s + a_o = 0$$

$$a_2 = \frac{-\alpha_f \lambda_f - \alpha_p \lambda_p + \beta \lambda_f}{\beta}$$

$$a_1 = \frac{-\alpha_f \lambda_f \lambda - \alpha_p \lambda_p (\lambda + \lambda_f)}{\beta} \qquad (7)$$

$$a_o = \frac{-\alpha_p \lambda_p \lambda \lambda_f}{\beta}$$

First harmonic perturbation

$$s^2 + \left[\frac{(\beta - \alpha_f)\lambda_f + \mu_1^2 M^2 (\lambda + \lambda_f)}{\beta + \mu_1^2 M^2} \right] s + \frac{(\mu_1^2 M^2 - \alpha_f)\lambda \lambda_f}{\beta + \mu_1^2 M^2} = 0 \qquad (8)$$

Figure 8 shows the values of the power coefficient and of the pressure coefficient that correspond to the stability limits. Values of the reactor parameters were assumed as follows: λ_f is 1 sec^{-1}, λ_p is 0.1 sec^{-1}, and λ is 0.1 sec^{-1}. The product, $\mu_1^2 M^2$, is 0.02 and corresponds to a heavy-water-moderated reactor that is 15 feet long in one linear dimension and in which the power distribution is flattened over approximately 40% of the linear dimension. The solid lines in Figure 8 give the stability limits for a value of β of 0.008, which corresponds to a fresh charge. The dashed line shows the limit for a value of $\beta = 0.004$, which would be approached at long fuel exposure when a substantial fraction of the reactor power would be obtained from fissions in plutonium.

The design point for the du Pont boiling reactor fueled with assemblies consisting of four concentric metal tubes is also shown on Figure 8. It is seen that this design is in the unstable region for the power level although it would be stable with respect to the power distribution. The design point can move to the right or left with changes in pump characteristics, steam quality, or fuel assembly design. For example, the design point corresponds to 30% steam quality and an α_f of 0.0088. If the steam quality were reduced to 15%, α_f would be 0.013. The point can move up or down with changes in the volume of the steam drum. A twofold decrease in the volume of the steam drum would move the point down to $\alpha_p = -0.0024$.

b. Transient Response by Numerical Integration

The boiling-D_2O-cooled reactor system was represented by the model shown in Figure 9 in the numerical integration computations of the

transient response of the system. The set of equations derived from this model was coded for solution on an IBM 650 computer. The response of a metal-fueled system to small perturbations in reactivity, as computed by numerical integration, confirmed the degree of instability indicated by the transfer function analysis.

(1) Description of Equations - The average fuel temperature, T_1 (^oC), is computed from the following rate equation

$$H_1 \frac{dT_1}{dt} = \lambda_1 \psi - \lambda_2 (T_1 - T_2) \qquad (1)$$

where λ_1, the fraction of total power generated in the fuel, is taken as unity (i.e., power generation in the moderator is ignored). For a steady-state pile power of ψ^o = 1220 MW, an assumed steady-state fuel temperature of 370°C, and a steam temperature of 270°C, λ_2 = 12.2 MW/°C. The heat capacity of the 63.8 tons of natural uranium in the core is H_1 = 7.51 MW-sec/°C. The quantity, T_2, is the temperature of boiling D_2O (^oC) at the system pressure.

Five groups of delayed neutrons are used:

$$\frac{d\mu_i}{dt} = \lambda_1 (1 + k_{ex})\phi - \lambda_i \mu_i \qquad (2)$$

The properties of the delayed neutron groups are shown in the table below.

Properties of Delayed Neutron Groups

i	Decay Constant, λ_i	Fraction, β_i
1	3.19 sec^{-1}	0.000324
2	1.19	0.000904
3	0.1997	0.004206
4	0.02469	0.0017133
5	0.0001305	0.000016516
	β	0.007163816

In Equation (2), μ_i is the concentration of the i^{th} delayed neutron precursor relative to its initial equilibrium value, and ϕ is the neutron flux relative to its initial equilibrium value.

The demineralizer and regenerative heater are merged into a single heat capacity block, and the temperature of the D_2O emerging from this block is given by

$$H_5 \frac{dT_5}{dt} = F_2(T_4 - T_5) \tag{3}$$

where F_2 is the flow rate in MW/°C into the demineralizer and H_5 = 78.9 MW-sec/°C.

The number of moles, n, of steam in the steam separators is computed from

$$\frac{dn}{dt} = \frac{F'x'}{m} - \frac{F_2'}{m} - \frac{V_{2\ell}\rho_\ell C}{hm} \frac{dT_2}{dt} \tag{4}$$

where m = 20 gm/mole, h = 345 cal/gm vaporized, C = 1.131 cal/gm-°C, F' = total flow through core = 1.777 x 10^6 gm/sec, F_2' is the flow rate in gm/sec of steam from the separators, x' is weight fraction of steam in the mixed phases entering the separators, $V_{2\ell}$ is the volume of D_2O in the separator sumps = 3.68 x 10^6 cm^3, and ρ_ℓ is the density of D_2O in gm/cm^3.

The pressure in the steam separators is given by

$$\frac{dP}{dt} = \frac{R(T_2 + 273.2)}{V_{2s}} \frac{dn}{dt} + \frac{nR}{V_{2s}} \frac{dT_2}{dt} \tag{5}$$

where R is the gas constant and V_{2s} is the gas volume in the steam separators (8600 ft^3), and where

$$\frac{dT_2}{dt} = \Delta T_2/\Delta t \tag{6}$$

Δt being the time increment used in the numerical integration of the differential equations.

The weight fraction, x', of steam in the mixed phases entering the separators is given by

$$\frac{dx'}{dt} = \lambda'(x - x') \tag{7}$$

where x is the weight fraction of steam in the mixed phases leaving the reactor and where the inverse transport lag time λ' in sec^{-1} is obtained from

$$\lambda' = F'/\bar{\rho}V_1 \tag{8}$$

Here, V_1 is the total piping volume between the core and the separators = 3.40 x 10^7 cm^3 and $\bar{\rho}$ is the density in gm/cm^3 of the mixed phases as given by

$$\bar{\rho} = \frac{S\rho_s\rho_\ell}{x\rho_\ell + S(1 - x)\rho_s} \tag{9}$$

The slip factor, S, has been taken as unity. The density of D_2O steam, ρ_s, is computed from

$$\rho_s = \frac{0.022285P}{T_2 + 273.2} \tag{10}$$

where P is the pressure in psi. The density of liquid D_2O, ρ_ℓ, in gm/cm^3 is computed from

$$\rho_\ell = C_o + C_1T_2 + \ldots + C_8T_2^8 \tag{11}$$

Two other loop D_2O equations are computed from differential equations

$$H_2 \frac{dT_2'}{dt} = F_1(T_2 - T_2') \tag{12}$$

$$H_2 \frac{dT_6'}{dt} = F(T_6 - T_6') \tag{13}$$

where the volume of the hot liquid return piping is 778 gallons, implying that H_2 = 10.4 MW-sec/°C, and the total volume of the pump suction piping, pumps, pump discharge piping, inlet collection header, and coolant inlet pipes is 4354 gallons, implying that H_6 = 62.2 MW-sec/°C.

The D_2O saturation temperature, T_2, is given in °C by

$$T_2 + 273.2 = a_o + a_1 \log P' + \ldots + a_7 \log^7 P' \tag{14}$$

where P' is the pressure in atmospheres.

Pile reactivity is computed from

$$k_{ex} = k(t) + k^* + \left(\frac{\partial k}{\partial \epsilon}\right)(\epsilon - \epsilon^o) + \left(\frac{\partial k}{\partial T_1}\right)(T_1 - T_1^o) \tag{15}$$

where k* represents the effect of control rod motion arising from an as-yet-unspecified feedback control system relating rod motion and electrical power demand and k(t) is the sum of all other externally imposed reactivity changes, such as that introduced by manually applied control rod motion. In Equation (15), ϵ is the average steam void fraction over the entire reactor core and is given by

$$\epsilon = (L_b/L)(\bar{\alpha}/\alpha)(\alpha) \tag{16}$$

where L_b/L is the fraction of the core in which boiling is occurring and $\bar{\alpha}/\alpha$ is the ratio of the average steam void fraction $\bar{\alpha}$ in the boiling portion of the core to the steam void fraction at the core exit α. The steam void coefficient of reactivity, $\partial k/\partial \epsilon$, multiplied by the change in the core-average steam void fraction, ϵ, from its initial equilibrium value, ϵ^o, yields the effect of steam voids on reactivity. The last term in Equation (15) takes into account the fuel temperature coefficient of reactivity. Since the moderator loop with its own heat exchanger is isolated from the core coolant loop, the moderator temperature has been assumed constant for the duration of rapid transients, and hence no moderator temperature coefficient of reactivity appears in Equation (15).

The relative flux, Φ, and the pile power, Ψ, in MW are related by

$$\Phi = \frac{\Psi}{\Psi^o} = \frac{\sum_{i=1}^{5} \beta_i \mu_i}{\beta(1 + k_{ex}) - k_{ex}} \tag{17}$$

The weight fraction, x, of steam in the mixed phases at the core exit is computed from

$$x = \frac{C\gamma_2(T_1 - T_2)}{hF} - \frac{C(T_2 - T_6')}{h} \tag{18}$$

and the corresponding steam volume fraction, α, at the core exit is

$$\alpha = \frac{x\rho_\ell}{x\rho_\ell + S(1 + x)\rho_s} \tag{19}$$

The fraction of the core in which boiling is occurring is computed from

$$\frac{L_b}{L} = \frac{hx}{hx + C(T_2 - T_6')} \tag{20}$$

The electrical power output, Ψ_e, from the turbine is assumed to be proportional to the steam flow, F_3, to the turbine

$$\Psi_e = \Psi_e^o(F_3/F_3^o) \tag{21}$$

The various steam flows are as follows:

$$F_3 = f_1 F_2 \tag{22}$$

$$F_4 = f_2 F_2 \tag{23}$$

$$F_5 = (1 - f_1 - f_2)F_2 \tag{24}$$

where the relative flow rates, f_1 and f_2, are input parameters.

The D_2O temperatures, T_4 and T_6, are obtained from

$$T_4 = \frac{T_3(F_3 + F_4)C + F_5(h + CT_2)}{CF_2} \tag{25}$$

where T_3 is the condenser outlet temperature, and

$$T_6 = \frac{F_2T_5 + F_1T_2'}{F} \tag{26}$$

The liquid D_2O flow, F_1, from the separators is simply

$$F_1 = F - F_2 \tag{27}$$

In the design, the following equilibrium values are specified:

$$F_1 = 9.9 \times 10^6 \text{ lb/hr}$$

$$F_2 = 4.2 \times 10^6 \text{ lb/hr}$$

$$T_3 = 41^\circ\text{C (assumed to be constant)}$$

$$T_2^\circ = 270^\circ\text{C}$$

$$\Psi^\circ = 1220 \text{ MW}$$

$$\Psi_e^\circ = 300 \text{ MW}$$

From these, the following equilibrium conditions can be derived:

$$x^\circ = x'^\circ = 0.2979$$

$$P^\circ = 814.66 \text{ psi}$$

$$n^\circ = 3.029 \times 10^5 \text{ moles}$$

$$\rho_s^\circ = 0.03342 \text{ gm/cm}^3$$

$$\rho_\ell^\circ = 0.8449 \text{ gm/cm}^3$$

$$\alpha^\circ = 0.9147$$

$$(L_b/L)^\circ = 0.6264$$

$$\epsilon^\circ = 0.4584$$

$$T_6^o = T_6'^o = 215.8^oC$$

$$T_4^o = T_5^o = 88.1^oC$$

$$T_2'^o = 270.0^oC$$

$$f_1 + f_2 = 0.9118$$

In addition, it is assumed that $f_1 = 0.90$ and $S = 1.0$.

(2) Transients Following a Step Reactivity Increase - Figure 10 shows the reactor power transients that follow a sudden reactivity increase of 0.001 k, for assumed values of the steam void coefficient of reactivity of -0.03, 0, and +0.03. In all three cases the fuel temperature coefficient of reactivity is taken as -2×10^{-5} $k/^oC$; the initial pile power is 1220 MW; the electrical power output (300 eMW) and the steam flow to the turbine (2.25 MW/°C) are held constant.

Evidently the system could be controlled if it had a zero or negative void coefficient; a positive void coefficient such as a value of +0.03, which is appropriate for natural uranium metal fuel, leads to an extremely severe power surge when the system is subjected to a sudden increase in reactivity.

With a constant steam flow from the separators, the pressure increases as the power rises. This increased pressure opposes the power surge by reducing the steam void volume. Figure 11 shows this effect to be much too small to be of any help. Even for a rather small $\Delta k = 0.00005$, the pile power climbs to over 3100 MW; operation at constant steam flow does in fact reduce the power level, as compared to operation at constant pressure, but does so to a significant degree only after the destructive power surge has occurred.

With a positive void coefficient of reactivity, there is a threshold value of $\partial k/\partial \epsilon$ below which oscillations in pile power, caused by changes in reactivity, are small and decay with time. Figures 12 and 13 show that, for a pile power of 1220 MW and a core exit steam quality of about 30%, this threshold $\partial k/\partial \epsilon$ has a value of +0.0167.

c. Conclusions Concerning Metal-Fueled Boiling D_2O Reactors

The preceding two articles have shown that a uranium-metal-fueled boiling-D_2O-cooled power reactor operating on a direct steam cycle will probably be unstable unless a very fast, foolproof feedback control system can be devised. It is doubtful that any simple changes in the reactor parameters, fuel element design, or reactor system will overcome this stability problem. Although these conclusions are subject to confirmation by measurements of the void and temperature coefficients, there is little likelihood that they will be invalidated by the

experimental data. Thus, it appears now that natural uranium metal fuel elements will find application only in liquid-(or gas-) cooled power reactors.

2. Machine Code for Computing Lattice Buckling

A code was written for the IBM 650 to calculate lattice bucklings by use of the method described in the SRL contributions to the 1958 Geneva Conference[2]. The input data required are the lattice geometry, type of fuel assembly, moderator temperature, lengths of fuel and end caps, and, for tubular assemblies, the size and composition of each region within the fuel assembly.

At present, only the lattice parameters for tubular assemblies can be computed with the code. The next step in this study will be to extend the code to permit machine calculation of the lattice parameters for clusters of solid rods. This latter calculation will employ the approximation of Carlvik and Pershagen[3] for the effective surface for resonance absorption of the clusters. The code will subsequently be extended to include the calculation of the lattice parameters for parallel plate assemblies.

a. Buckling

The buckling, B^2, is obtained from the critical equation,

$$k = (1 + L^2B^2)(1 + \tau_1 B^2)e^{\tau_2 B^2} \qquad (1)$$

Equation (1) may be solved for B^2 as a polynominal in $z = (k - 1)/M^2$,

$$B^2 = z - Fz^2 + 2F^2z^3$$

where

$$F = \left[L^2\tau + \tau_1\tau_2 + \frac{1}{2}\tau_2^2\right]\Big/M^2 \qquad (2)$$

$$M^2 = L^2 + \tau$$

$$\tau_1 = a_1\tau$$

$$\tau_2 = (1 - a_1)\tau$$

$$k = \eta\epsilon pf$$

In the above equations and those below the following nomenclature is used:

k = multiplication factor

B^2 = buckling

L^2 = diffusion area

τ = neutron age

τ_1 = "age" of fast neutrons

τ_2 = "age" of epithermal neutrons

M^2 = migration area

η = neutron reproduction factor

ϵ = fast fission factor

p = resonance escape probability

f = thermal utilization

a_1 = 0.378 for D_2O

Definitions of other symbols are given in the text as they are encountered.

b. Thermal Utilization and Diffusion Area

Values for the thermal utilization, f, and the diffusion area, L^2, are obtained from the already available P-3 code for calculating the flux distribution in cylindrical lattice cells. At present, the P-3 input data sheet must be filled out to run a problem; however, a subroutine is being prepared to calculate the required P-3 input data directly from the input data required for this buckling code.

c. Thermal Neutron Reproduction Factor

At present, the thermal neutron reproduction factor, η, is assumed to be a constant, 1.327, for all lattices.

d. Fast Fission Factor

The convention used in calculating ϵ, the fast fission factor, is that all fissions in U^{238} are included in ϵ but the associated (n,γ) reactions are included in p. Thus

$$\epsilon = 1 + \frac{\gamma_f - 1}{\gamma_{th}} \delta = 1 + a_2\delta \qquad (3)$$

where δ is the ratio of the number of fissions in U^{238} to the number in U^{235}. The values for γ_f and γ_{th} in natural uranium are taken as 2.51 and 2.46, respectively.

A family of curves was presented in Reference 2 that gave δ as a function of the radius of the fuel assembly and of the relative amounts of D_2O, U, and Al. These curves were obtained using the modification of Spinrad's method[2].

In this method, all of the material inside the outer uranium surface, or inside a surface defined by a rubber band stretched around the outer uranium surfaces, is homogenized. If the volume of this region is V_a, its effective radius is $r_a = (V_a/\pi)^{1/2}$. The family of curves for δ was fitted with the equation

$$\delta = \left[1 - (0.725 - 0.225f_u)f_a\right]\left[0.0491 + 1.2116f_u + 0.622f_u^2\right] \times \left[0.0057 + 0.02057r_a - 0.001133r_a^2\right] \quad (4)$$

In Equation (4),

$$f_u = V_u/(V_u + V_D)$$

$$f_A = V_A/(V_u + V_D + V_A) = V_A/V_a$$

V_u, V_D, and V_A are the volumes of uranium, water, and structural materials, respectively, in the homogenized region.

e. Neutron Age

The expression used for τ, the neutron age, is

$$\tau = \left[120 - 400\, f_N^{(7)}\right]\left[1 - \frac{V_E}{V_T} - \frac{1}{2}\frac{V_u}{V_T}\right]^{-2} \quad (5)$$

where $f_N^{(7)}$ is the atom fraction of H_2O in the moderator, V_T is the total cell volume, V_E is the total volume of structural materials and voids in the cell, and V_u is the uranium volume. This expression yields τ for 20°C water and must be multiplied by the square of the ratio of the density of water at 20°C to that at the cell temperature, T. At present this can be accomplished in the code by replacing 120 by $120\left[\frac{\rho(T)}{\rho(20)}\right]^2$ as part of the input. A calculation of the density of D_2O as a function of T is being incorporated.

f. Resonance Escape Probability

In the Geneva paper[2], the resonance escape probability, p, is assumed to be linear in the fractional absorption rate,

$$\Delta p = A\Phi_c \frac{N_1 V^{(1)}(RI)}{(\bar{\xi}\Sigma_s)(V^{(6)} + V^{(7)})} \quad (6)$$

where

(RI) = resonance integral

$\overline{\xi\Sigma}_s$ = macroscopic slowing down power

N_1 = number of fuel atoms per cc

$V^{(1)}$ = total volume of natural uranium in cell

$V^{(6)}$ = total volume of D_2O in cell

$V^{(7)}$ = total volume of H_2O in cell

Φ_c = flux ratio (defined below)

A = normalization constant (explained below)

The code has been made a little more flexible by defining p as

$$p = 1 - \Delta p + a_3(\Delta p)^2 + a_4(\Delta p)^3 \tag{7}$$

The SRL recipe given at Geneva is reproduced by taking $a_3 = a_4 = 0$; an exponential dependence is obtained by taking $a_3 = 1/2$, $a_4 = -1/6$.

The correction for the fact that resonance flux is lower far out in the moderator than it is near a source that does not absorb many resonance neutrons was expressed by Critoph[4] and in the SRL recipe as a sum of the contributions to the resonance flux from neighboring assemblies. In the present calculation this sum is replaced by the ratio, Φ_c, of flux in the center of the cell to the average flux in the cell, as given by the expression,

$$\Phi_c = 1 + 0.0089 \left[\left(\frac{\tau_L}{\tau_M} \right)^{1/2} s - 6.2 \right]^2 \tag{8}$$

where

$$\left(\frac{\tau_L}{\tau_M} \right)^{1/2} = \left[1 - \frac{V_E}{V_T} - \frac{1}{2} \frac{V_u}{V_T} \right]^{-1} \tag{9}$$

and s is the triangular lattice spacing in inches.

In the SRL Geneva paper, the denominator of Δp contained the total volume of the cell. This has been replaced with the total volume of water in the cell, $V^{(6)} + V^{(7)}$. The value of $(\overline{\xi\Sigma}_s)$, the slowing down power of the moderator, is taken as

$$(\overline{\xi\Sigma}_s) = 0.370\, f_N^{(6)} + 1.53\, f_N^{(7)} \tag{10}$$

where N indicates the outermost region.

The resonance integral that is used for uranium is of the form

$$RI = \frac{a}{G_o} + b\left(\frac{S_e}{M}\right) + c\left(\frac{S_e}{M}\right)^2 \qquad (11)$$

where S_e is the effective surface of the assembly in cm^2 per unit length and M is the mass in grams per unit length. Values of a, b, and c were quoted in the Geneva paper.[2] These constants should now be different for two reasons. Originally they were obtained to optimize the agreement between the calculated bucklings and a series of central hex measurements in the PDP. These measurements have since been corrected. In addition, the constants were derived using the total volume of the cell in the denominator of Δp and the substitution of the water volume for the total volume will cause changes in these constants. The constants will be re-evaluated by comparing measured and calculated bucklings.

The mass is

$$M = 18.9\left[V^{(1)} + a_5 V^{(2)}\right] \qquad (12)$$

where a value of a_5 of 0.46 is used and $V^{(1)}$ and $V^{(2)}$ are the total volumes of uranium metal and uranium oxide in the cell, respectively. The effective surface is

$$S_e = S_1 + \frac{1}{G_o}\left[E_c S_2 + \sum_i E_{si} S_{3i}\right] \qquad (13)$$

where S_1 is the outer surface for tubes or the rubber band perimeter for plates or clusters. For tubes, S_2 is the interior surface of the innermost tube and S_{3i} is the sum of the two surfaces facing coolant annulus number i. The quantity, E_c, is the effectiveness of the inner surface for resonance energy absorptions as given by

$$E_c = \frac{4y^2}{3}\left[(2y + y^{-1})K_1(y)I_1(y) + 2yK_o(y)I_o(y) - 2\right.$$
$$\left. - K_o(y)I_1(y) + K_1(y)I_o(y)\right] \qquad (14)$$

where y is the reduced radius

$$y = \frac{1}{r_b \lambda}\sum_{n=1}^{n_b} \beta_M(n)\left[r_n^2 - r_{n-1}^2\right] \qquad (15)$$

The sum is taken over all regions inside the innermost fuel region; $\beta_M(n)$ is the value of λ^{-1} in material M divided by 0.351, the value of λ^{-1}, the reciprocal of the transport mean free path in heavy water. The effectiveness for slabs, $E_s = [1 - 2E_3(t\lambda^{-1})]$, is used for the effectiveness of the tubular surfaces separated by annuli, where E_3 is

the collision probability function for slabs and t is the slab thickness. In the range of interest, E_s is accurately fitted by the polynominal

$$E_{si} = 1.85x_i - 2.00x_i^2 + 1.00x_i^3 \tag{16}$$

where x_i is the reduced thickness, which for the case of two tubes only is given by

$$x_i = \frac{1}{\lambda(r_{a-1} - r_{b+1})} \sum_{n=n_{b+2}}^{n=n_{a-1}} \beta_M(n) \left[r_n^2 - r_{n-1}^2 \right] \tag{17}$$

For other cases it is only necessary to change the limits of summation.

The quantity, G_o, corrects for the flux dip of resonance energy neutrons within the fuel assembly. It is the ratio of flux at the outer surface to average flux in the fuel. To obtain G_o, the assembly is divided into 3 homogeneous regions. Region I extends from r = 0 to $r = r_b$, the inner radius of the inner fuel tube. Region II extends from $r = r_b$ to r_a where r_a is the outer radius of the outer fuel tube. Region III extends from r_a to the outer cell radius, r_N. The flux shape is obtained by solving the diffusion theory equations,

$$D_I \nabla^2 \phi_I - (\bar{\xi}\Sigma_{sI}/\Delta\ell)\phi_I + q_I = 0 \tag{18}$$

$$D_{II} \nabla^2 \phi_{II} - \Sigma_{aII} \phi_{II} = 0 \tag{19}$$

$$D_{III} \nabla^2 \phi_{III} - (\bar{\xi}\Sigma_{sIII}/\Delta\ell)\phi_{III} + q_{III} = 0 \tag{20}$$

where D is the diffusion coefficient, $\bar{\xi}\Sigma_s$ is the slowing down power of the moderator, Σ_a is the macroscopic absorption coefficient, $\Delta\ell$ is the effective lethargy interval of the resonance absorption region in uranium, and q is the neutron source term.

The usual boundary conditions of zero current at the cell center and edge and of continuity of flux and current at the two interfaces are applied. This gives numerical values for the constants, B and C, in

$$\phi_{II}(r) = BI_o(\kappa_{II} r) + CK_o(\kappa_{II} r) \tag{21}$$

Then,

$$\phi_s = \phi_{II}(r_a) \tag{22}$$

$$\bar{\phi} = \frac{2\pi}{\kappa_{II} V_{II}} \left[Br_a I_1(\kappa_{II} r_a) - Br_b I(\kappa_{II} r_b) - Cr_a K_1(\kappa_{II} r_a) + Cr_b K_1(\kappa_{II} r_b) \right] \tag{23}$$

and

$$G_o = \phi_s / \bar{\phi} \tag{24}$$

To solve the diffusion equations it is necessary to supply the ratio, v, of q_I to q_{III}. This is assumed to be

$$v = \frac{V_I^{(6)} + V_I^{(7)}}{V_I} \Bigg/ \frac{V_{III}^{(6)} + V_{III}^{(7)}}{V_{III}} \tag{25}$$

Values of κ_1, the extinction coefficient and D_1, the diffusion coefficient or, what is equivalent, values of Σ_s, Σ_{tr}, Σ_{abs}, and $\bar{\xi}$ the macroscopic cross sections for scattering, transport, absorption, and the average logarithmic energy decrement per collision, respectively, for each material are supplied within the code; they are not required for each problem.

In the expression for Δp, A is a parameter that can be adjusted to obtain agreement between calculated and measured bucklings. Its primary use is in calculating bucklings for a series of similar assemblies, the buckling of one of which has been measured. It is intended that A be determined for an experimental assembly and then be used for calculating p and B^2 for other similar assemblies.

g. Calculation of Volumes and Surfaces

The volumes and surface areas required for the above equations are calculated from the diameters provided as input data for each region. At present this section is programmed only to handle tubular assemblies. It is planned to extend the programming to handle clusters of rods and bundles of plates. The only changes that will be required in the main part of the code are in the equations for surface effectiveness.

3. Shielding Experiments

Many of the current designs for D_2O-moderated power reactors require internal thermal shields composed of various mixtures of iron and D_2O. The effects of such shields are quite complex and involve the slowing down and capture of fast neutrons, the absorption of slow neutrons, and the attenuation of both the pile gammas and the gammas resulting from neutron capture in the shield itself. While these processes have been studied extensively for iron-H_2O mixtures, almost no experimental work has been done on iron-D_2O mixtures. In order to partially fill this gap in the data, a few experiments were performed on a candidate iron-D_2O shield in the Shielding Studies Tank of the Process Development Pile (PDP) at the Savannah River Laboratory.

The PDP shield test facility consists of a stainless steel tank, 70 inches high, 74 inches wide, and 40 inches thick, positioned against the outer

wall of the PDP at the vertical midplane of the pile. The shield tank covers approximately a 50° sector of the PDP tank wall. A diagram of the shield facility is shown in Figure 14. During the experiments described here, 49% of the volume of the front half of the tank was occupied by "Duriron" grid blocks.

Two series of measurements were made during the course of the D_2O shielding experiments. One series compared the effects of D_2O (99.16 mol %) and H_2O in attenuating the pile leakage flux passing through the shield tank. The other series determined the neutron age for Po-Be neutrons in the shield tank. Different tank fillings and source positions were used to obtain age values for D_2O and H_2O as well as for the various iron-water ratios.

a. Attenuation of the PDP Leakage Radiation in the Shield Tank

In the first set of experiments the PDP was loaded with an unreflected lattice of natural uranium rod clusters in D_2O. Leakage neutrons from this lattice had a cadmium ratio for gold pins of approximately 3.7 at the tank wall. The effectiveness of the shield in attenuating these leakage neutrons was determined by irradiating gold and indium foils placed throughout the shield tank. In the inner half of the shield the foils and pins were taped to 2S aluminum strips and inserted at the positions shown in Figure 14. Spacers were used at these positions to keep the foils approximately 0.5 inch from the iron. In the outer half of the shield tank a special frame constructed with 2S aluminum strips was used to hold the foils.

A plot of the relative flux distribution through the reactor and the shield tank, as obtained from the gold pins and foils, is shown in Figure 15 for both the D_2O and H_2O tank fillings. The distribution from the indium foils are shown in Figures 16 and 17.

The accuracy of these measurements as determined from average counting statistics varied from ±5% for the foils nearest the pile to ±50% for the foils in the lowest flux region in the center of the shield. Essentially only the measurements made in the inner half of the shield tank have any meaning. Because the shield covers only a small portion of the PDP tank, a large fraction of the PDP leakage is emitted without attenuation and some sizeable portion of this attenuated flux is reflected into the shield tank. The outer half of the tank serves primarily as a shield against the reflected radiation. Likewise all measurements are made at the center line of the shield tank to eliminate the effects of reflected radiations at the sides and top. The magnitude of this effect can be determined from the flux rise at the outer wall of the shield tank.

Gamma ray attenuation through the shield tank was determined from photographic film exposures with H_2O in the tank. The results are shown in Figure 18. No such measurements have as yet been made with D_2O.

However, the gamma ray attenuation coefficient, as distinct from the gamma source distribution, should be essentially identical for both the D_2O and H_2O fillings.

b. Neutron Age

The age of Po-Be neutrons was determined for the various ratios of iron and water used in the inner half of the shield tank by measuring the spatial distribution of the neutron slowing down density at the 1.4-ev resonance of indium. In the same manner, the age was measured in the outer half of the shield tank for both H_2O and D_2O (99.16 mol %) for comparison with previously reported values[5]. Because it was difficult to establish the effective boundaries of the mixtures, different source positions were used. In this way the possible boundaries and, thus, the value of τ were bracketed. These positions were: (1) the inner water space between the "Duriron" and the wall of the tank, (2) the wet side of the outer wall, and (3) the space between the double wall spacer between the inner and outer half of the shield tank.

In terms of the foil activities, τ in spherical coordinates can be expressed as

$$\tau \text{ (to 1.4 ev)} = \frac{r^2}{6} = \frac{4\pi \int r^4 A(r)dr}{24\pi \int r^2 A(r)dr} \qquad (1)$$

where r is the distance from the source to the detector and A(r) is the measured activity. In order to use this expression in evaluating τ from the data, the logarithm of the foil activities, A, was plotted against r. A smooth curve was drawn through the experimental points. This curve was then used to aid in the construction of the curve, ln Ar^2 against r. Also, in the cases in which the counting statistics were very poor, the logarithm of the product A'r was also plotted against r, where A' is the activity of the bare indium foils. The slope of A'r vs. r was used to extrapolate the ln Ar^2 vs. r curve for values of r greater than 30 cm.

The experimental curve of ln Ar^2 against r was extrapolated to infinity by assuming that the slowing down density was proportional to $\frac{e^{-r/\lambda}}{r^2}$ at distances greater than 30 cm. The slope, λ, of the extrapolated portion of the curve was determined by weighting the accuracy of the experimental points and the slope of the line drawn for the curve, ln $A'r^2$ vs. r.

The extrapolated curve of ln Ar^2 vs. r was then used to construct plots of Ar^2 and Ar^4 against r. The areas under these curves were measured with a planimeter and the values thus obtained were used for the integrals in Equation (1).

The experimental results are given in Table I. The errors in τ listed in the table were estimated from the statistical error in the foil counts and the uncertainty in the extrapolated portion of the curves. The following values of the neutron age were obtained by averaging the values given in Table I.

Neutron Age to 1.4 ev, Po-Be Neutrons

	Current Experiments	DP-163[5]
H_2O	68 cm^2	56 cm^2
D_2O (99.16 mol %)	151 cm^2	148 cm^2
H_2O-"Duriron" 1:1 by volume	77 cm^2	--
D_2O-"Duriron" 1:1 by volume	215 cm^2	--

Although these values for the age are somewhat higher than those previously measured, presumably because of the poor geometry of the shield tank, the agreement was regarded as satisfactory for the purposes of these experiments.

B. REACTOR FUEL MATERIALS

1. Fuel Elements of Uranium Metal

a. Thin Tubes for Irradiation Testing

Work has been started at Nuclear Metals on the development of modified fabrication techniques to permit the production of thin tubes of uranium metal for irradiation testing. Several billets of Zircaloy-clad unalloyed uranium are being assembled for experimental extrusions to determine the optimum extrusion temperature and to explore the effects of various core-end shapes. Information from this study should assure that tubes can be produced within specifications for cladding thickness, especially in the area of the core-end tapers. Concurrently, full-scale tubes of unalloyed uranium are being extruded, with billet designs based on the best information available from previous work.

Two types of core-end shapes, "spherical" and "angular", were incorporated in two tubes extruded early in April. Subsequent autoradiographic and destructive evaluation revealed thinning of the outer cladding near both front and rear ends on the tube with the "spherical" core-end shape and thinning of only the outer cladding near the front end on the tube with the "angular" core-end shape. Accordingly, the latter design, with a slight modification of the front, was used for a subsequent set of three tubes. Autoradiography of one of these tubes showed that there was still some thinning of the outer cladding on the front end, as well as slight thinning of the inner cladding. The processing of this tube will be completed to permit its use for flow testing at Savannah River. Evaluation of the other two tubes is not yet complete.

Two additional tubes of the thin-walled design, with U - 1.5 wt % Mo and U - 1 wt % Si cores, respectively, were extruded as prototypes for tubes desired for irradiation testing at Vallecitos. Evaluation of these tubes is in progress, to determine whether the designs used will be satisfactory for fabrication of similar tubes with 3% enriched uranium cores.

b. Swelling of Uranium-Base Alloys

As was reported in DP-495, an experimental program has been initiated at the Savannah River Laboratory to characterize the metallurgical behavior of uranium and some of its alloys during irradiation at power reactor temperatures. The objective of the program is to define the causes and possible means of control of fuel swelling. In this program, Zircaloy-clad tubes of uranium about 8 inches long will be irradiated in lead-insulated capsules of stainless steel in a Savannah River reactor. Progress during May in the preparation of these irradiation specimens is reviewed below.

Zircaloy-clad tubes with cores of U - 2 wt % Zr and U - 1.5 wt % Mo were successfully coextruded to the required dimensions. Billets are now being prepared for extruding the irradiation specimens. The first group will contain unalloyed uranium. The billet cores for these tubes will be machined from a heavy-walled tube that was pre-extruded from a forged billet. The coextruded tubes will be sealed at the ends by counterboring to remove the exposed uranium and inserting a Zircaloy end plug, which will then be welded to the sheath to complete the closure. Excellent welds were obtained at these joints with the SRL electron beam welder. A cross section of a typical weld is shown in Figure 19.

The capsule for the tubular specimens is a tube that will be water-cooled on both the inside and outside surfaces. The specimens will be enclosed in stainless steel cans formed by welding end plugs in the annulus formed by two concentric tubes. The most desirable heat transfer conditions require a 0.060-inch annulus of lead on the inside surface of the specimen and a 0.122-inch annulus on the outside surface. Three dummy assemblies were made to test the feasibility of preparing such a capsule. Both annuli of each assembly were filled with lead along the entire length of the 7.5-inch specimen. Longitudinal and transverse sections of the completed capsule are shown in Figure 20. The bottom end plug and top spacer that were used in the experiment maintained the desired concentricity.

The encapsulation was performed in a vertical tube furnace that was so arranged that the specimen could be lowered at a controlled speed through the furnace. First, a predetermined amount of lead was melted in the can. When the lead was molten, the specimen, with top spacer attached, was inserted in the can. When the specimen centered itself on the conical bottom end plug, the assembled capsule was slowly

lowered from the furnace to obtain directional freezing. The result was that the shrinkage cavity formed at the top of the capsule, where heat transfer was not important. An inert atmosphere over the molten lead was necessary to avoid the formation of lead oxide during the encapsulation.

c. Creep and Stress-Rupture Studies of Fuel Cores

Measurements of the mechanical properties of unalloyed uranium and U - 1.5 wt % Mo are being made at Nuclear Metals to determine whether the differences in properties of these two materials can be related to differences in their irradiation behavior. Under irradiation the dimensional stability of the U - 1.5 wt % Mo alloy has been much superior to that of the unalloyed uranium. The measurements that will be made under this study will include (1) short-time tensile tests at room temperature as well as at elevated temperatures and (2) creep tests at various temperatures and initial stresses. The unalloyed uranium test specimens were beta heat treated; the U - 1.5 wt % Mo specimens were given a special heat treatment consisting of 15 minutes at 775°C, a furnace cool to 620°C, one hour at 620°C, and then an air cool to room temperature in the evacuated heat-treatment container. This latter heat treatment produces in extruded material a microstructure resembling that of the "as-cast" alloy.

Short-time tensile tests to date have shown that U - 1.5 wt % Mo is considerably stronger than unalloyed uranium at temperatures up to about 550°C. The ductility of the U - 1.5 wt % Mo increases with temperature. Uranium, on the other hand, was anomalous in its behavior; the elongation at rupture decreased continuously from 28% at 150°C to 18% at 500°C, and these specimens were deformed over the full gage length.

Creep and stress rupture data have also been obtained for U - 1.5 wt % Mo, but are not yet available for unalloyed uranium. The results for both materials will be reported when the tests on the unalloyed cores are complete.

d. Studies of Zircaloy Cladding for Metal Fuel Elements

A study has been in progress at Nuclear Metals to evaluate the factors that may determine the service life of Zircaloy-clad fuel elements by affecting the strain limit of the cladding and/or the core. Last month, in DP-495, a summary was included of the experimental results obtained from burst tests of samples of cladding, core, and cladding-core composite, representing various fabrication parameters. The results of subsequent metallographic examinations are now available to aid in interpretation of the experimental observations.

The recent test results indicate that the ductility of unalloyed uranium in the beta-treated condition is improved (from 6 to 15% fracture strain) by the standard acceptance corrosion test for clad

specimens, i.e., 24 hours in 340°C water plus 24 hours in 400°C, 1500 psi steam. This thermal treatment causes a reduction of the average grain size from 120 to 85 microns. This grain refinement and the stress relief that probably accompanies the recrystallization appear to be a reasonable explanation for the observed increase in ductility.

The burst tests indicated a limited ductility (8% fracture strain) for specimens of Zircaloy-clad U - 2 wt % Zr in the diffusion-heat-treated condition. In contrast, the core alone, tested in the same metallurgical condition, gave 18% fracture strain. Also, during burst testing of the clad specimens, cracks were formed at the cladding-core interface, and these cracks led to dimpling of the cladding. Metallographic examination of these specimens revealed a diffusion zone between cladding and core that was about 0.0055 inch thick and comprised four or five bands. In this zone were large cracks parallel to the tube axis; the cracks were widest in the diffusion zone, but many of them penetrated into the core. These observations indicate that the low ductility of the diffusion zone is probably the factor limiting the ductility of these diffusion-heat-treated fuel tubes.

2. Fuel Elements of Uranium Oxide

a. Vibratory Compaction Plus Swaging

Equipment for experimental study of the vibratory compaction of fuel elements of uranium oxide was put into service at the Savannah River Laboratory. This equipment consists of an MB Electronics Co. Vibrator (Model C-10) and a Model T-151 amplifier. When oxide tubes were compacted in this equipment, the number of subsequent swaging passes to achieve a final density of nearly 90% was reduced from twelve to a maximum of six. Six tubes with stainless steel cladding were loaded with -20 mesh Norton fused UO_2; the tubes were vibrated at 550 to 625 cps with an acceleration of 20g. Densities after vibratory compaction ranged from 70 to 76% of theoretical density. The tubes were swaged to final densities that ranged from 85.3 to 89.5% of the theoretical density, as shown in Table II.

Vibratory compaction and a new hydraulic feeder for the swager produced the smoothest tube surfaces achieved to date.

b. Improvement of Vibratory Compaction

Initial experiments with vibratory compaction were conducted to determine the optimum distribution of particle size for high packing densities of fused UO_2. Although tubular elements are the desired shape, rods were used in these experiments. Both tubular and rod elements have shown maximum settling at the resonant frequency (between 400 and 650 cps for both 2-foot pieces and 4-foot pieces). The maximum density attained was not dependent upon the acceleration, but the rate of settling was greater at higher accelerations.

The particle size distributions of "as-pulverized" -20 mesh Spencer fused UO_2 or Norton fused UO_2 did not result in a satisfactory increase in packing density in the vibratory compaction rod specimens. However, considerable improvement was obtained by blending various particle sizes in special mixtures. These results are shown in Table III. The maximum density achieved thus far was 88%, which was obtained with a mixture containing 58.0% of -10/+16 mesh particles, 15.2% of -70/+100 mesh particles, and 26.8% of -200 mesh particles. These data will be applied to the compaction of tubular specimens.

C. IRRADIATION TESTS

1. Coextruded Tube of Unalloyed Uranium in NRU Reactor

The Zircaloy-clad tube of unalloyed uranium that is being irradiated in the E-20 loop of the NRU reactor at Chalk River was removed from the reactor for interim examination after reaching an average exposure of 750 MWD/T and a maximum exposure of 950 MWD/T. Results of this examination were generally satisfactory; the maximum volume increase was less than 1.5%, and the strain in the outer cladding was 0.14%. In view of this satisfactory behavior, it was decided to continue the irradiation. Mechanical difficulties not related to fuel behavior precluded immediate reinsertion of the element, but plans are being made to correct these difficulties so that the test can be resumed at an early date.

a. Tube Description and Operating Conditions

The purpose of the irradiation test is to obtain data on the dimensional stability of tubes of unalloyed uranium under irradiation conditions approximating those predicted for D_2O-moderated power reactors. The nominal dimensions of the coextruded tube were as follows:

Outside diameter	2.070 inches
Inside diameter	1.467 inches
Cladding thickness (Zircaloy-2)	0.030 inch
Over-all length	11 feet
Effective core length	8.9 feet

A typical set of operating conditions are:

Reactor power	200 MW
Total power output of loop	935 KW
Power output of fuel	885 KW
Maximum specific power	22.9 MW/T
Maximum heat flux	275,000 pcu/(hr)(ft^2)
Maximum-to-average flux ratio	1.265
Coolant flow	202 gpm

Loop pressure	1090 psig
Coolant inlet temperature	177°C
Coolant outlet temperature	196°C
Maximum surface temperature	250°C
Maximum core-clad interface temperature	335°C
Maximum core temperature	400°C

During this initial exposure, the conditions outlined above were maintained so that the maximum metal temperature during full-power operation was held to 400 ±5°C. Eight thermal cycles (trips or scrams) were experienced; the duration of these cycles ranged from 5 to 40 minutes.

b. Postirradiation Measurements

Volume Changes - Diameters were measured at a number of inspection stations along the length of the fuel tube by means of a Dixie Gauge. The Dixie Gauge is an underwater device whose main component is a linear differential transformer, the signal from which is transformed into a direct reading of diameter. These measurements and the resultant calculated volume changes are shown in Table IV together with the fuel exposure and calculated temperatures at each station. The temperatures are based on a maximum metal temperature of 400°C. These diameter and volume changes are also plotted in Figure 21. As seen in this figure, a fair amount of scatter was observed because of the small magnitude of the changes in diameter. The real changes in diameter are most likely represented by the smooth curves in Figure 21. On this basis, it is concluded that the maximum volume change is between 1.0 and 1.5%.

A comparison of the behavior of this tube with that of a U - 2 wt % Zr tube irradiated at Vallecitos (see DP-475) shows no significant difference in the amount of volume change for the same exposures. There is, however, a significant difference in the manner by which these two tubes increased in volume. The outside diameter of the Vallecitos tube changed about 3.5 times as much as did the inside diameter, but in the NRU tube the change in outside diameter was no more than one-half the change in inner diameter.

Based on a maximum increase of 0.003 inch in the outside diameter (Station 14 in Table IV), the maximum strain in the outer cladding of the NRU tube is 0.14%, which is well within the performance limit normally considered acceptable for conditions such as those of this test.

Surface Appearance - Prior to irradiation, the surface of the element was characterized by slight undulations most easily observed by oblique light. These surface undulations extended over the entire length of fuel and probably occurred during the beta heat treatment. With proper lighting, the undulations were observed in the

postirradiation examination with no noticeable change except over the end seals, where some minor additional rippling apparently occurred. The surface after irradiation was black and shiny with no sign of film buildup.

2. Slugs of U - 2 wt % Zr

Four Zircaloy-clad slugs of U - 2 wt % Zr were inspected visually after being irradiated to modest exposure at uranium temperatures in the range of interest for D_2O-moderated power reactors. The four slugs, which were clad with 0.005 to 0.025 inch of Zircaloy-2, were irradiated in a Savannah River reactor with the objective of obtaining data on the effects of cladding thickness and exposure on the dimensional stability of the U - 2 wt % Zr alloy. The irradiation conditions for these slugs and the results of similar tests on eight other slugs are reported in DP-340.

The inspection revealed that one end cap had separated from the slug that had 0.005 inch of cladding. The separation was at the core-cap interface. This is the second instance of end cap separation on a slug with 0.005 inch of cladding. No cracks were detected in the cladding over the cores of the slugs. A more detailed inspection of the slugs will be made at higher magnification, and dimensions will be measured after the cladding is cleaned.

3. Swaged Tubes of Uranium Oxide

The assembly of swaged oxide tubes that failed during irradiation in a Savannah River reactor (see DP-485) was disassembled, the location and nature of the failure were established, and preparations were made for metallurgical examination of the failed element. The assembly contained five tubes of uranium oxide that were swaged in stainless steel cladding with welded end closures. Each tube was 2.14 inches in OD, 1.46 inches in ID, and 2 feet long. Measurements of radioactivity release from the individual tubes revealed that the third element in the column of five was the one that had failed. A photograph of the failure is shown in Figure 22. The failure was in the form of a 9-inch-long crack in the outer cladding at a position opposite one of the ribs of the housing tube. Apparently, little or no uranium oxide escaped.

Although the cause of the failure is unknown, several hypotheses have been advanced. The most probable causes are (1) internal steam formation following "waterlogging", and (2) volume increases produced by conversion of UO_2 to U_3O_8; either of these modes of failure requires the presence of an initial cladding defect. Such defects might have existed in the welded closures, might have been introduced in the tube wall by the cold swaging operation, or might be ascribed to the use of "Weldrawn" stainless steel tubing; however, tests of swaged tubing from the same lot indicated that the metal is ductile and the weld is sound. Other hypotheses ascribe the rupture to thermal expansion of the oxide, water

originally present in the element, corrosion of the cladding, or buildup of fission gas pressure.

4. Swaged Rods of Uranium Oxide

Postirradiation examination of four swaged rods of arc-fused UO_2 clad in stainless steel and irradiated in the MTR revealed no appreciable changes in specimen dimensions (Table V) or in general appearance. The rods were punctured and the fission gases were collected for analysis by mass spectrograph.

The rod assembly was irradiated in reflector position A-39 in the MTR. The estimated fuel power ranged from 10.2 KW/ft at the reactor midplane to 2.2 KW/ft near the top of the core. The calculated maximum burnup was 4460 MWD/T of uranium. The power and burnup values summarized in Table V are based on a peak unperturbed thermal flux of 1.15×10^{14} $n/(cm^2)(sec)$ as reported by MTR personnel and on a typical flux pattern for a similar test position. These values are tentative and subject to correction or confirmation by the postirradiation burnup analyses.

5. Stainless Steel Weld Metal

Comparative irradiation tests of stainless steel weld metal and of parent plate showed that welds in Type 304 stainless steel have higher yield strength and lower ductility than does the parent plate, both before and after irradiation to fast neutron exposures as high as 1.2×10^{21} n/cm^2. The effects of irradiation on the tensile properties and the hardness of weld specimens are summarized in Figures 23 through 26.

The specimens that were used in these experiments were machined from 5/8-inch plate of Type 304 stainless steel that was butt-welded with Type 308 filler metal according to du Pont standard engineering specifications. The longitudinal axes of the specimens of weld metal and of the heat-affected zone were in the direction of the weld line. The parent plate was in the "as-rolled" condition prior to welding. The specimens were irradiated while immersed in high purity D_2O at a temperature of less than 100°C. Fast neutrons are defined here to include all those with energies greater than 0.1 Mev.

D. JOINTS OF ZIRCALOY AND STAINLESS STEEL

One of the chief problems that must be faced in the design of pressure tube power reactors is that of joining pressure tubes of Zircaloy to coolant distributors of stainless steel. A bonded joint is thought to be a potentially better solution to this problem than is a mechanical joint because the former is more compact. Therefore, a program was undertaken at Nuclear Metals, Inc., under a du Pont subcontract to develop a suitable process for fabrication of a bonded joint. The progress of this program was discussed in DP-445 and in subsequent

progress reports. This article describes the fabrication process that was developed at Nuclear Metals and recapitulates the various tests that have been performed on joint specimens.

1. Fabrication Process

The bonded joints produced at Nuclear Metals are prepared by extruding stainless steel and Zircaloy in tandem in the stated order. Prepared billets of the two materials are etched, assembled into an evacuated can, and extruded at 870°C. After the extruded specimen is cooled, it is machined to final dimensions. The shapes of the billet and the extruded joint are shown in Figure 27.

The principal process variables are as follows:

a. Temperature - Extrusion temperatures of 815, 870, and 900°C were tried with equally good results. At 815°C, the stainless steel was stiffer than was desired, while at 900°C the thickness of the bond layer was excessive. The intermediate temperature was selected as the process standard although temperature control appeared not to be a particularly critical factor.

b. Ram Speed - The ram speed was varied from 13 inches per minute to 140 inches per minute without noticeable effect on the extrusion. The lower speed was selected as the standard speed.

c. Reduction in Area - Extrusion ratios of 6 and 10 were investigated. No difference in results between the two was noted, but it is thought that the higher ratio may produce more reliable results.

d. Cooling After Extrusion - Although it had been thought that rapid postextrusion cooling would be helpful in minimizing growth of the diffusion layer, an investigation of water quenching and air quenching indicated that the quench method does not have a detectable effect on the diffusion layer.

e. Bond Layer - The use of titanium and niobium as interface materials to facilitate bonding between the Zircaloy and the stainless steel was investigated. The titanium produced a low-strength joint that had poor corrosion resistance. The niobium joint also exhibited poor corrosion resistance. In view of these findings, the use of interlayers was discontinued.

f. Types of Material - All of the development work thus far has been with joints containing austenitic stainless steels; no stainless steels in the 400 series have been investigated. Most of the development has been with Types 304L and 347; Type 304 has been used in a few rod extrusions with good results. Zircaloy-2 has been used for all joints fabricated to date.

2. Characteristics of the Joint

Evaluation tests indicate that the properties of the tandem-extruded joints are as follows:

a. Strength - By proper control of the geometry of the extrusion billets, the joint interface is a taper that is 8 to 12 inches long. With such an interface, the operating stresses at the joint are chiefly shear stresses. Tensile tests show that the strength of the joint is greater than that of the Zircaloy-2. All of the failures in some 25 tensile specimens occurred in the Zircaloy-2, which exhibited strength values of 30,000 to 50,000 psi.

b. Bond Thickness - The thickness of the diffusion bond is 0.0001 to 0.0002 inch.

c. Brittleness - Although the interface layers are more brittle than the parent metal, this does not appear to be disadvantageous. A tensile test of a joint specimen that was rolled to 20% reduction in area resulted in fracture of the Zircaloy-2 rather than the bond. No separation occurred at the interface when longitudinal strips from a 2-inch-OD tubular joint were subjected to 360° bend tests.

d. Corrosion Resistance - In 28-day corrosion tests of several specimens in water at 360°C, there was no evidence of preferential corrosion at the joint interface. This test is estimated on the basis of Zircaloy weight gain to be equivalent to 8 years of exposure to water at a service temperature of about 250°C. Bond strengths of other joint sections were measured by performing stud-weld tests after a 14-day corrosion test of the sections in water at 360°C. The exposure to elevated temperature apparently did not adversely affect the bond strength.

e. Fatigue - Two tubular joints successfully withstood a 116-cycle test in which they were internally pressurized with water at a maximum temperature of 260°C and a maximum pressure of 1000 psi. Metallurgical examination of the joints after completion of the cyclic tests disclosed no distortion and no corrosion.

f. Cracks - No cracks were detected in joints that were examined at a magnification of 1500.

E. HEAVY WATER LEAKAGE

The mechanical seal assembly on the outboard end of a centrifugal pump in a flow loop at the Savannah River Laboratory was recently modified so that the rate of leakage of water vapor from the seal could be measured. As discussed in previous reports, the vapor leakage from mechanical seals is of interest in the design development of D_2O-moderated power reactors because such leakage is not readily recoverable.

During the first 6 hours of operation at a pump suction pressure of 850 psig, the maximum vapor leakage from the test seal assembly was less than 0.02 lb/yr of water, which is insignificant. The measurement of liquid leakage from both the inboard and outboard seals of the test pump is continuing. The liquid leakage during 103 days of operation averaged 350 lb/yr from the inboard seal and 730 lb/yr from the outboard seal. The pump, which is driven at 3600 rpm by a 200-hp motor, is used to recirculate deionized water at a maximum flow of 2800 gpm and at 260°C in the test loop.

The outboard seal and bearing assembly of the the test pump and a flow diagram of the liquid and vapor collection systems are shown in Figure 28. Any vapor that leaks past the throttling ring in the seal flange is swept out of the vapor collection chamber by a metered stream of dry nitrogen. The vapor leakage is then measured by analyzing the effluent stream of nitrogen for moisture. A positive pressure of about 2 inches of H_2O is maintained in the liquid and vapor collection systems to prevent inleakage of air. Leakage rates between 0.005 and 50 lb/yr can be measured with the moisture-detecting instrument.

The average vapor leakage from a mechanical seal on the outboard end of the bench-scale seal test equipment discussed in DP-495 was 7 lb/yr of H_2O during a 55-hour test at a shaft speed of 3600 rpm and at a pressure of 1000 psig. The average liquid leakage from the seal during this period and at the same conditions was 200 lb/yr of H_2O. A "Durametallic" mechanical seal for a shaft diameter of 2.63 inches was used for the test. An identical seal except for a shaft diameter of 2.00 inches was also tested at the same time on the inboard end of the tester. However, on the latter seal only the liquid leakage was measured, because it was not practical to modify the test apparatus for measuring vapor leakage. The average liquid leakage from the inboard seal at the above conditions was 510 lb/yr of H_2O. The leakage collection systems were almost identical with those discussed above and shown in Figure 28; the mechanical design of the "Durametallic" seals was also similar to that of the seal on the centrifugal pump.

F. HEAT TRANSFER

1. Burnout Heat Flux of Roughened Surfaces of Zircaloy

The measured burnout heat flux of a water-cooled surface of Zircaloy-2 that was intentionally roughened with a diamond knurl pattern was 40% higher than that of a smooth Zircaloy surface at the same coolant conditions. The friction factor for the roughened surface was 1.8 times that of the smooth surface. These measurements were made as part of a program to determine whether a significant increase in heat transfer limits for fuel assemblies in a liquid-D_2O-cooled reactor can be realized by mechanical roughening of the cladding surface. Although the experiments were conducted at pressure levels which are well below those of interest for power reactors, it is not expected that the effect of surface roughening on the burnout heat flux will be greatly different at higher pressures.

The results of burnout tests on two knurled specimens of Zircaloy-2 are shown in Table VI. Similar data for smooth specimens were presented in DP-445. The burnout heat flux for the knurled specimens was about 10% lower than that of a knurled surface of stainless steel at the same friction factor. The tests were made with electrically heated tubes of Zircaloy-2 that were 0.50 inch in diameter and 24 inches long. The heated specimen formed the inner surface of an annulus and was cooled with subcooled water. The outer surface of the annulus was formed by a smooth housing tube of glass. The Zircaloy-2 that was used for the tests on rough surfaces was not etched or autoclaved.

2. Design of Fuel Assemblies Cooled by Boiling D_2O

At present, the design of fuel assemblies for a boiling D_2O reactor is hampered by lack of adequate experimental data on heat transfer burnout and hydraulic characteristics for flow of boiling water. Experimental programs at the Savannah River Laboratory and at Columbia University are directed toward obtaining such information in sufficient quantity to make reliable designs of fuel assemblies. In the meantime, available calculational methods are being used as a basis for appraising candidate fuel assemblies for irradiation in the boiling D_2O loop of the HWCTR. The results of the application of these methods to concentric-tube assemblies and to clusters of rods are summarized in Tables VII and VIII, and are discussed in the following paragraphs. These results indicate that a satisfactory distribution of boiling coolant can be achieved in both types of fuel assembly from the standpoint of uniformity of steam quality.

The flow distribution in the fuel assemblies was calculated by the method outlined in DP-445. This method treats a steam-water mixture as a homogeneous fluid, the properties of which are obtained by weighting the properties of the two phases according to their relative mass. The applicability of this method to flow in individual tubes has been verified at pressures of about 100 psi.

The two types of assemblies presently being considered for irradiation in the boiling D_2O loop of the HWCTR are (1) two concentric tubes of metallic uranium, and (2) a bundle of 19 rods of uranium oxide. Both of these assemblies were described in DP-485. The concentric-tube design contains three coolant annuli that are not interconnected along their length. They all have the same total pressure drop, the same exit pressure, and the same inlet subcooling. Once the heat release to each annulus and the total coolant flow are specified, the division of flow in the element can be calculated by matching the pressure drops in the individual annuli. The exit steam qualities can then be calculated. The results of these calculations at nominal operating conditions for the boiling D_2O loop are shown in Table VII. These data indicate that the design described in DP-485 provides adequate coolant distribution (Design I in Table VII). Uniform steam quality could be achieved by decreasing the diameter of the housing tube, but this design change is not regarded as essential for purposes of HWCTR irradiation tests.

The basic rod bundle design that was considered in the calculations is composed of 0.55-inch-diameter rods on 0.633-inch centers. The inner seven rods are arranged hexagonally, while the peripheral twelve rods are arranged on a circle. In the calculations for the 19-rod bundle, the total cross section for coolant flow was divided into three regions, as follows:

Inner region - bounded by the central rod and the hexagon defined by the centers of the six middle rods.

Middle region - bounded by the hexagon defined by the centers of the six middle rods and by the circle defined by the centers of the twelve peripheral rods.

Outer region - bounded by the circle defined by the centers of the twelve peripheral rods and by the housing tube.

These three regions were treated as though they were not interconnected, i.e., it was assumed that no crossflow of coolant could occur between the regions. This assumption is questionable, particularly since the rods are spaced by helical ribs which may promote mixing of coolant. Otherwise, the calculations were the same as those for the concentric-tube assembly. The results are presented in Table VIII. It is seen that the indicated distribution of coolant is poor for the 19-rod bundle in a circular housing tube. Better coolant distributions could be obtained by using a scalloped housing tube to eliminate some of the cross section for flow in the outer region, or, alternatively, by substituting a dummy rod for the central fuel rod to reduce the heat input to the inner region.

BIBLIOGRAPHY

1. St. John, D. S., et al. Preliminary Hazards Evaluation of the Heavy Water Components Test Reactor (HWCTR). E. I. du Pont de Nemours & Co., Aiken, S. C. AEC Research and Development Report DP-383, 181 pp. (1959).

2. Driggers, F. E. and D. S. St. John. "Physics of Natural Uranium, Heavy Water Reactors." Dietrich, J. R. and W. H. Zinn. Solid Fuel Reactors. Massachusetts: Addison-Wesley Publications (1958) pp. 432-58.

3. Carlvik, I. and B. Pershagen. The Dancoff Correction in Various Geometries. Aktiebolaget Atomenergi, Stockholm, Sweden. AE-16, 23 pp. (1959).

4. Critoph, E. Comparison of Theory and Experiment for a) Lattice Properties of D_2O-U Reactors, b) Central Rod Experiments, and c) Foreign Rod Experiments. Atomic Energy of Canada, Ltd., Chalk River, Ontario, CRRP-655, 63 pp. (1956).

5. Wade, J. W. "Neutron Age in Mixtures of D_2O and H_2O." Nuclear Sci. and Eng. 4, 12-24 (1958); Neutron Age in Mixtures of Light and Heavy Water. E. I. du Pont de Nemours & Co., Aiken, S. C. AEC Research and Development Report DP-163, 35 pp. (1956).

TABLE I

SUMMARY OF AGE MEASUREMENTS IN PDP SHIELDING TANK

Source Position	Mixture	τ to 1.4 ev Po-Be Neutrons, cm^2	Estimated Error, cm^2	Area $A_s r^2$, x 10^6 cm^3		Area $A_s r^4$, x 10^9 cm^5		Per Cent Area $A_s r^4$ Extrapolated	λ, cm
				Total	Extrapolated Portion	Total	Extrapolated Portion		
Front	D_2O-Iron	214	±25	70.92	15.84	90.85	60.6	67	16.6
Center	D_2O-Iron	216	±20	138.65	32.1	179.9	120.9	67	18.4
Front	H_2O-Iron	85	±10	79.65	4.95	4.05	1.4	34	11.2
Center	H_2O-Iron	63	±10	17.36	0.67	7.28	1.92	26	9.6
Rear	D_2O	168	±25	184.7	32.7	186.6	113.9	61	15.9
Center	D_2O	161	±20	132.5	22.4	106.1	67.1	58	15.1
Rear	H_2O	79	±10	13.41	0.55	6.4	1.70	27	9.6
Center	H_2O	56	±10	12.76	0.375	4.31	1.00	23	9.7

TABLE II

DENSITIES OF OXIDE TUBES PREPARED BY VIBRATORY COMPACTION AND SWAGING

UO_2 Density After Vibratory Compaction, % of Theoretical	UO_2 Final Density, % of Theoretical[(a)] Area Reduction During Swaging, %			
	8	17	21	26
70.0	76.9	89.8	86.4	88.4
72.1	78.6	87.5	87.3	89.5
72.7	79.3	87.5	87.8	
72.1	78.9	87.3	87.6	
76.2	83.0	88.8		
73.2	80.0	85.3		

(a) Final densities were approximated from tube diameters and elongation, which may account for the nonuniform density increase. Density measurements are in progress.

TABLE III

VIBRATORY-COMPACTED DENSITY OF OXIDE RODS MADE FROM BLENDS OF VARIOUS PARTICLE SIZES

Weight Per Cent of Indicated Size Fraction[(a)]									UO_2 Density, % of Theoretical
-20	-6/+10	-10/+16	-20/+40	-40/+70	-70/+100	-120/+200	-200	-325	
100%	-	-	-	-	-	-	-	-	71.6
80%	20%	-	-	-	-	-	-	-	76.5
60%	40%	-	-	-	-	-	-	-	79.6
40%	60%	-	-	-	-	-	-	-	73.1
-	50%	-	30%	-	-	15%	-	5%	80.4
-	40%	-	35%	-	-	20%	-	5%	82.8
-	30%	-	40%	-	-	20%	-	10%	83.0
-	60%	-	-	15%	-	-	25%	-	84.7
-	-	58.0%	-	-	15.2%	-	26.8%	-	88.0

(a) Size distributions are shown in terms of U. S. standard sieve series.

TABLE IV

VOLUME CHANGES IN ZIRCALOY-CLAD TUBE OF UNALLOYED URANIUM
After Irradiation in E-20 Loop of NRU Reactor

Stn. No.	Inches from Bottom Tip of Fuel	Temperatures, °C: Central Metal	Clad Interface	Clad Surface	Coolant	Exposure, MWD/T	Average Diameter Change, mils: Outside	Inside	Per Cent Volume Increase
4	2	278	247	205	177	380	0.8	+1.5	-0.08
5	8	312	271	216	177	595	-0.1	-0.2	0.02
6	14	335	286	224	178	680	1.6	-1.8	0.70
7	20	360	300	230	178	745	0.4	-2.3	0.51
8	26	370	310	235	179	810	1.2	-2.3	0.70
9	32	382	319	240	180	860	0.9	-5.0	1.1
10	36	388	324	243	181	895	1.2	-5.2	1.2
11	40	392	328	244	182	915	0.9	-3.9	0.91
12	44	398	331	246	183	935	1.8	-5.3	1.4
13	48	400	334	247	184	945	1.8	-6.0	1.5
14	52	400	335	250	185	955	3.0	-3.8	1.4
15	56	397	333	250	186	945		-3.0	
16	60	390	326	250	187	905		-4.0	
17	64	388	323	250	188	880		-3.6	
18	68	384	320	249	189	850	- Not measured	-2.1	- Unavailable
19	72	378	317	248	190	820		-3.6	
20	76	371	313	247	191	790		-2.3	
21	80	365	305	246	192	745		-2.8	
22	86	353	294	245	193	685		-1.8	
23	92	338	283	240	194	610		-1.2	
24	98	310	258	230	195	525		-1.2	
25	104	270	235	217	196	430		-1.2	
26	110	215	205	200	196	325		-0.7	

TABLE V

FABRICATION AND IRRADIATION DATA FOR RODS OF
SWAGED URANIUM OXIDE IN STAINLESS STEEL CLADDING

Specimen Number	Bulk Density, g/cm³	O/U Ratio	Power[a], KW/ft: Avg.	Max.	Burnup[a], MWD/T of U: Avg.	Max.	Estimated Central Temperature, °C[b]: Avg.	Max.	Diameter, in.[c]: Before	After	Length, in.: Before	After
428H	9.96	2.132	5.6	9.1	2460	3960	1140	2620	0.575 (.0010)	0.575 (.0015)	11.33	11.340
431C	9.86	2.087	9.6	10.2	4190	4460	1540	1680	0.575 (.0012)	0.575 (.0013)	6.12	6.129
428C	9.96	2.132	9.8	10.2	4280	4460	> 2760	> 2760	0.574 (.0012)	0.574 (.0009)	6.61	6.606
431H	9.86	2.087	6.0	9.4	2640	4100	760	1490	0.575 (.0009)	0.575 (.0016)	11.59	11.603

(a) The power and burnup levels are based on a peak unperturbed thermal flux of 1.15×10^{14} n/(cm²)(sec).
(b) The central temperatures were computed with a thermal conductivity function constructed by a least squares fit of the data of Hedge (AECU-3381). The correction to thermal conductivity for excess oxygen is $k(UO_{2+x}) = k(UO_2)[1-4.3x]$, which is based on data reported by Runnalls (CRL-55).
(c) Standard deviations in parentheses

TABLE VI

BURNOUT HEAT FLUX OF DIAMOND-KNURLED ZIRCALOY-2 SURFACE

Electrically heated specimens (0.5 in. dia. x 24 in. long) were cooled by liquid water; specimen surfaces were roughened by medium diamond knurls (235 points/in.^{2})

Run number	1	2
Depth of roughness, in.	0.015	0.015
Channel thickness, in.	0.187	0.187
Coolant velocity, ft/sec	14.9	15.0
Pressure, psia	50.7	49.6
Subcooling at burnout point, °C	63.8	41.0
Friction factor of rough surface divided by friction factor of smooth surface	1.78	1.80
Burnout heat flux, pcu/(hr)(ft^2)	1,500,000	1,300,000
Burnout heat flux for smooth Zircaloy-2 surface, pcu/(hr)(ft^2)	1,083,000	935,000
Ratio of burnout heat flux for rough surface to burnout heat flux for smooth surface at same velocity, pressure, and channel thickness	1.39	1.40

TABLE VII

HEAT TRANSFER IN CONCENTRIC-TUBE FUEL ASSEMBLIES COOLED BY BOILING WATER

Design		I[a]	II[b]
Housing ID, in.		2.494	2.45
Outer fuel tube	OD, in.	2.06	2.06
	ID, in.	1.70	1.70
Inner fuel tube	OD, in.	1.020	1.020
	ID, in.	0.660	0.660
Coolant mass velocity, lb/(sec)(ft^2)	Inner	545	613
	Middle	545	624
	Outer	545	512
Coolant flow, lb/hr	Inner	4,700	5,200
	Middle	19,800	22,700
	Outer	21,100	17,700
Steam quality, %	Inner	14.1	12.2
	Middle	14.5	12.2
	Outer	9.7	12.2
Pressure drop, psi		10.6	11.7

Power = 1.43 MW
Coolant flow (H_2O) = 45,600 lb/hr
Pressure = 795 psia
Subcooling = 9°C
Tube length = 9.5 ft
Axial cosine flux distribution

(a) See DP-485
(b) Design I modified to yield equal exit steam qualities

TABLE VIII

HEAT TRANSFER IN FUEL ROD CLUSTERS
COOLED BY BOILING WATER

Design		I[a]	II[b]	III[c]	IV	V[b]
Housing shape		Circle	Circle	Circle	Scalloped	Scalloped
Number of fuel rods		19	18	18	19	18
Pressure drop, psi		12.5	12.8	10.9	20.5	20.8
Coolant mass velocity, lb/(sec)(ft^2)	Inner	280	382	770	490	650
	Middle	415	410	345	730	710
	Outer	630	620	515	550	535
Coolant flow, lb/hr	Inner	2,300	3,100	9,900	4,000	5,300
	Middle	13,600	13,400	11,300	23,900	23,200
	Outer	29,800	29,400	24,400	17,600	17,100
Steam quality, %	Inner	39.8	19.3	3.8	21.0	10.0
	Middle	20.1	22.1	27.0	10.3	11.3
	Outer	6.2	7.1	8.9	12.8	14.1

Power = 1.43 MW
Coolant flow (H_2O) = 45,600 lb/hr
Pressure = 795 psia
Subcooling = 9°C
Axial cosine flux distribution

(a) See DP-485
(b) No heat generation in the central rod
(c) Smaller central rod (D = 0.25 in.) with no heat generation

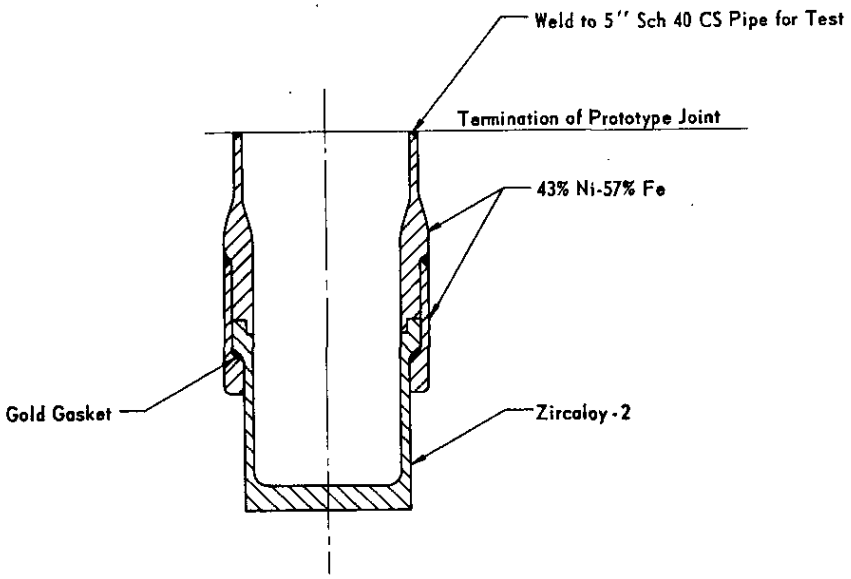

FIG. 1 PROTOTYPE OF ZIRCALOY-TO-STAINLESS-STEEL JOINTS FOR HWCTR BAYONETS

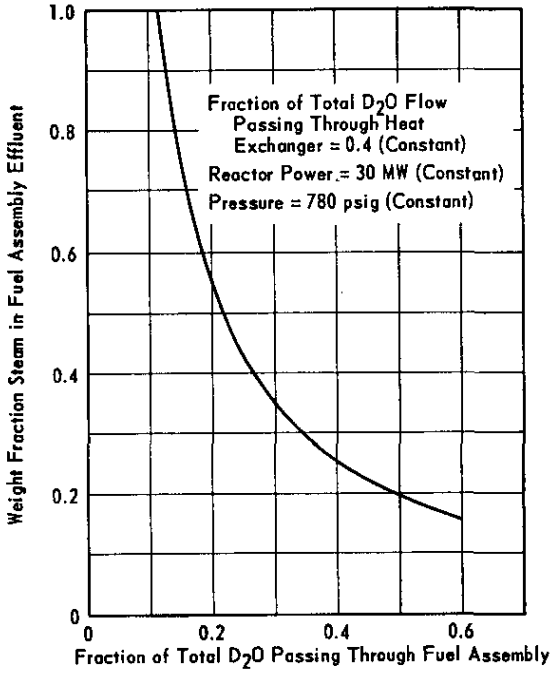

FIG. 2 STEAM QUALITY IN BOILING LOOP OF HWCTR AS FUNCTION OF D_2O FLOW THROUGH FUEL ASSEMBLY

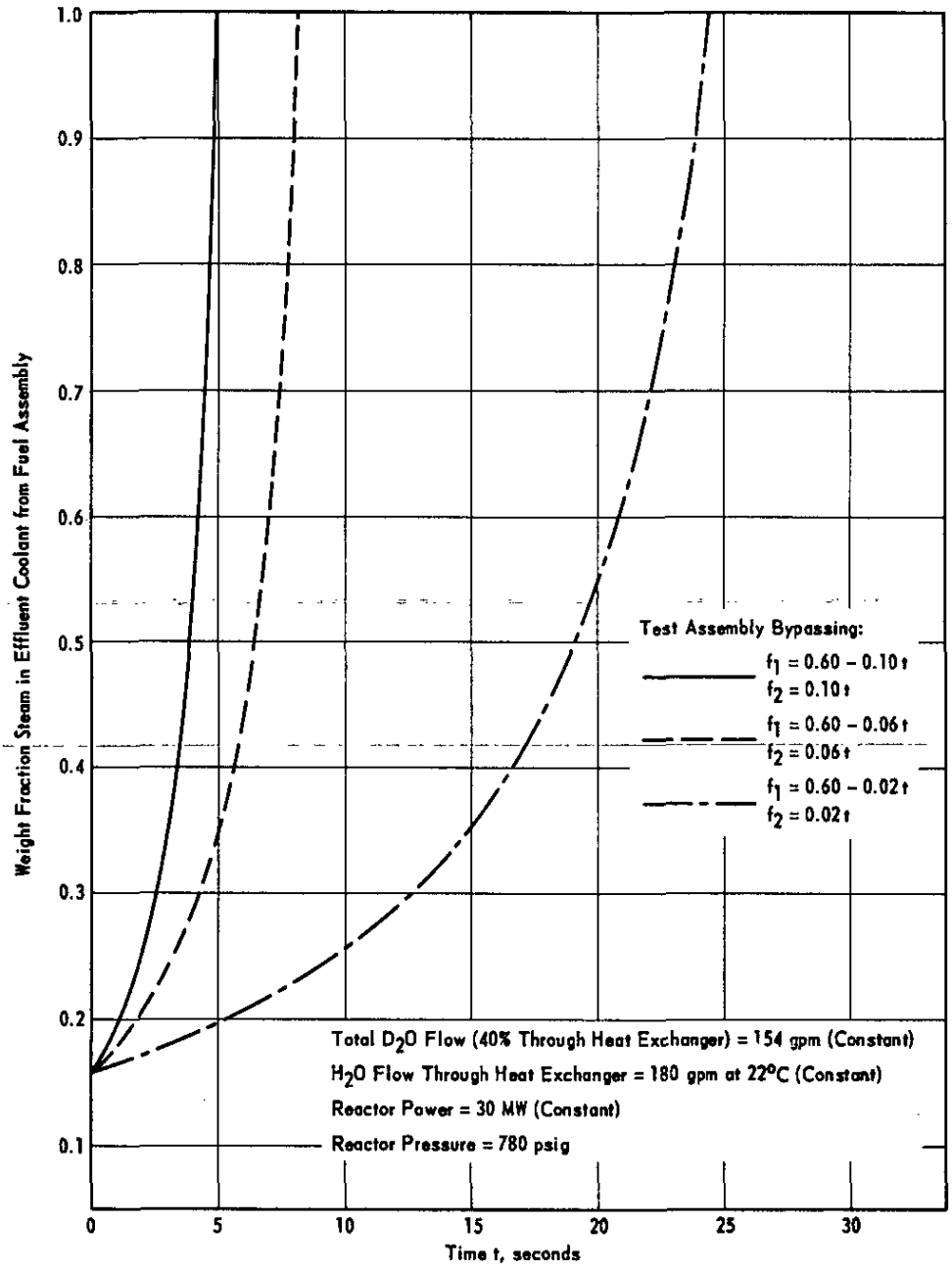

FIG. 3 EFFECT OF COOLANT BYPASS RATE ON STEAM QUALITY IN BOILING LOOP OF HWCTR

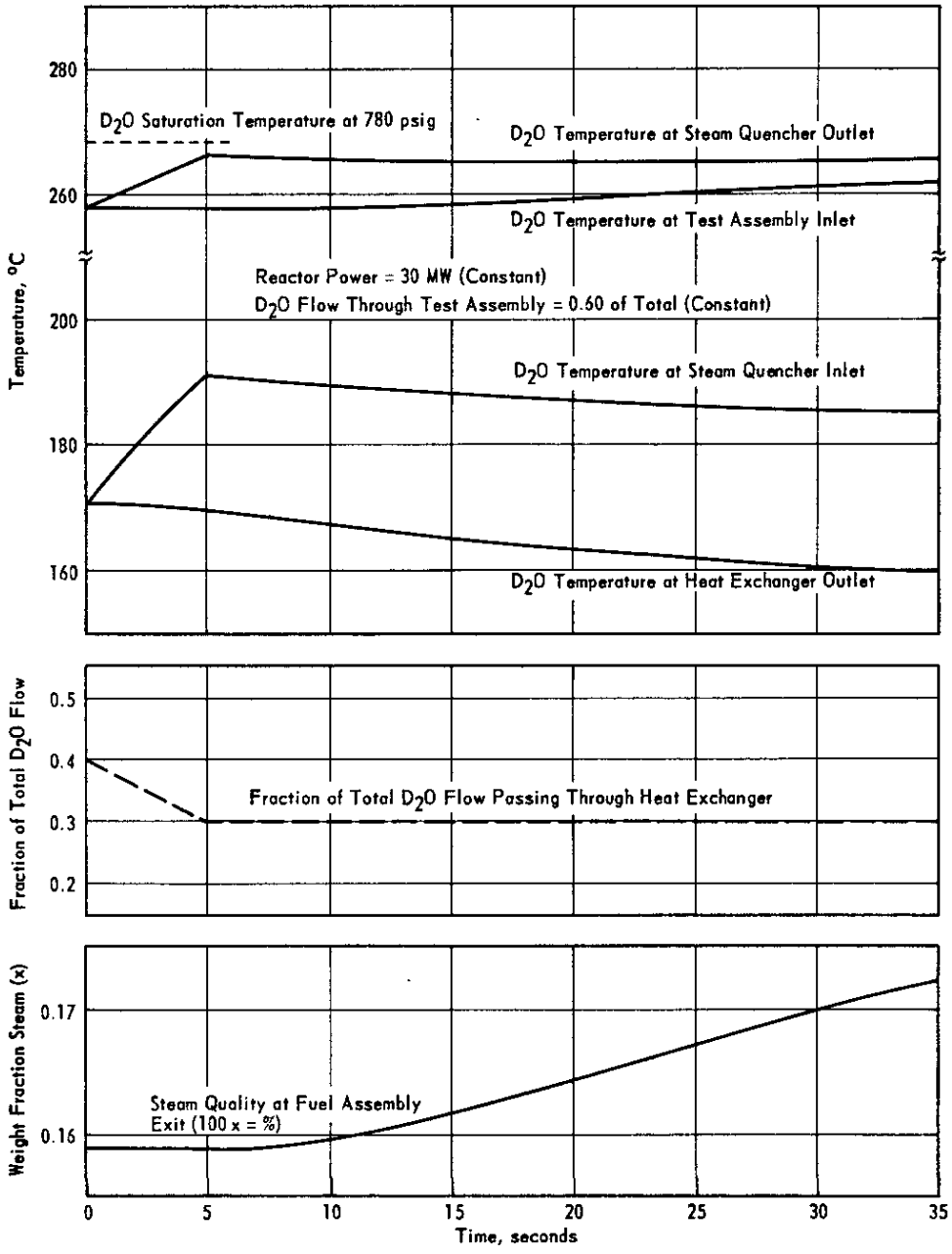

FIG. 4 TRANSIENT THERMAL EFFECTS OF PARTIAL BYPASSING OF HEAT EXCHANGER IN BOILING LOOP OF HWCTR

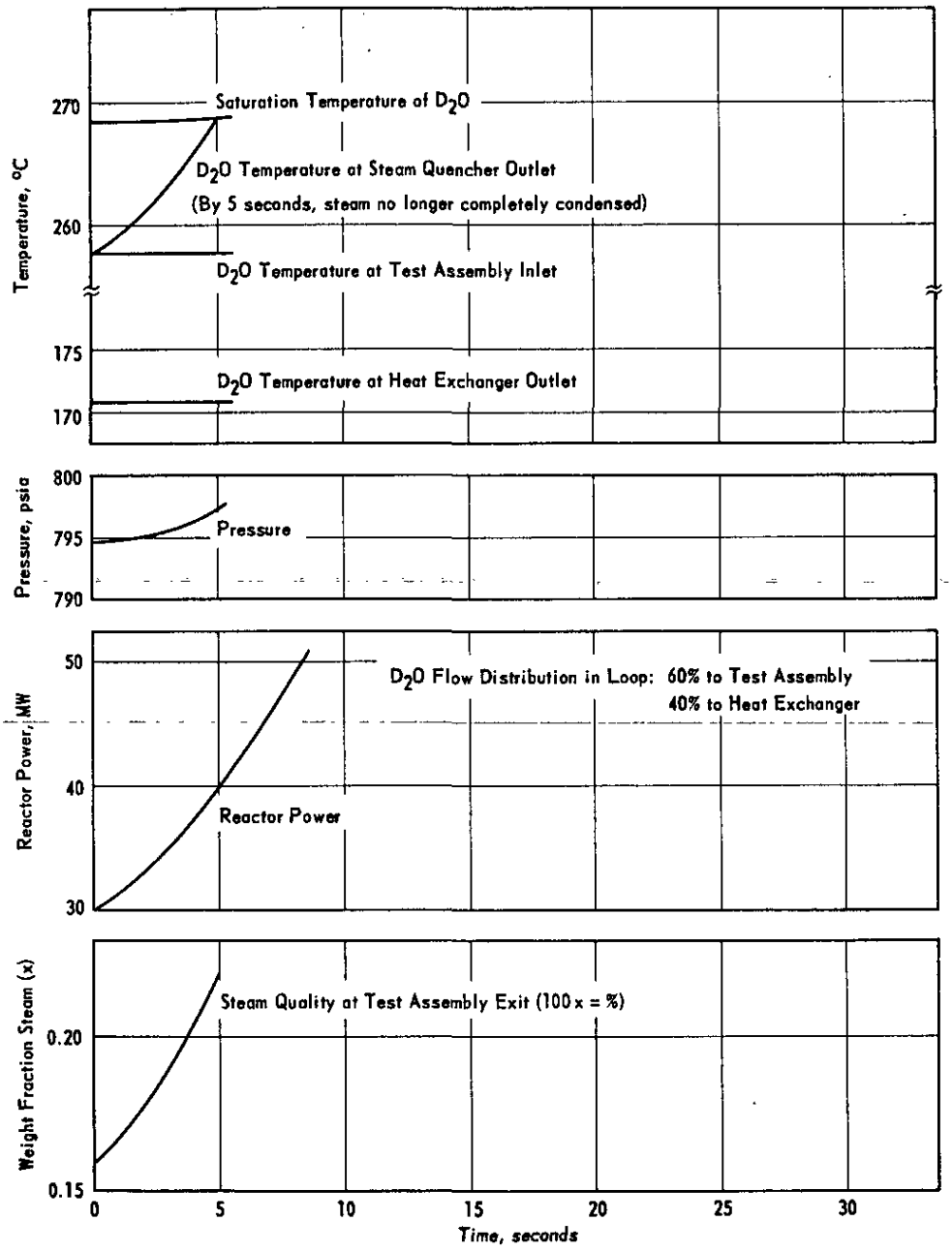

FIG. 5 TRANSIENT RESPONSE OF BOILING LOOP OF HWCTR TO RAMP ADDITION OF REACTIVITY AT 0.0003 k/SEC

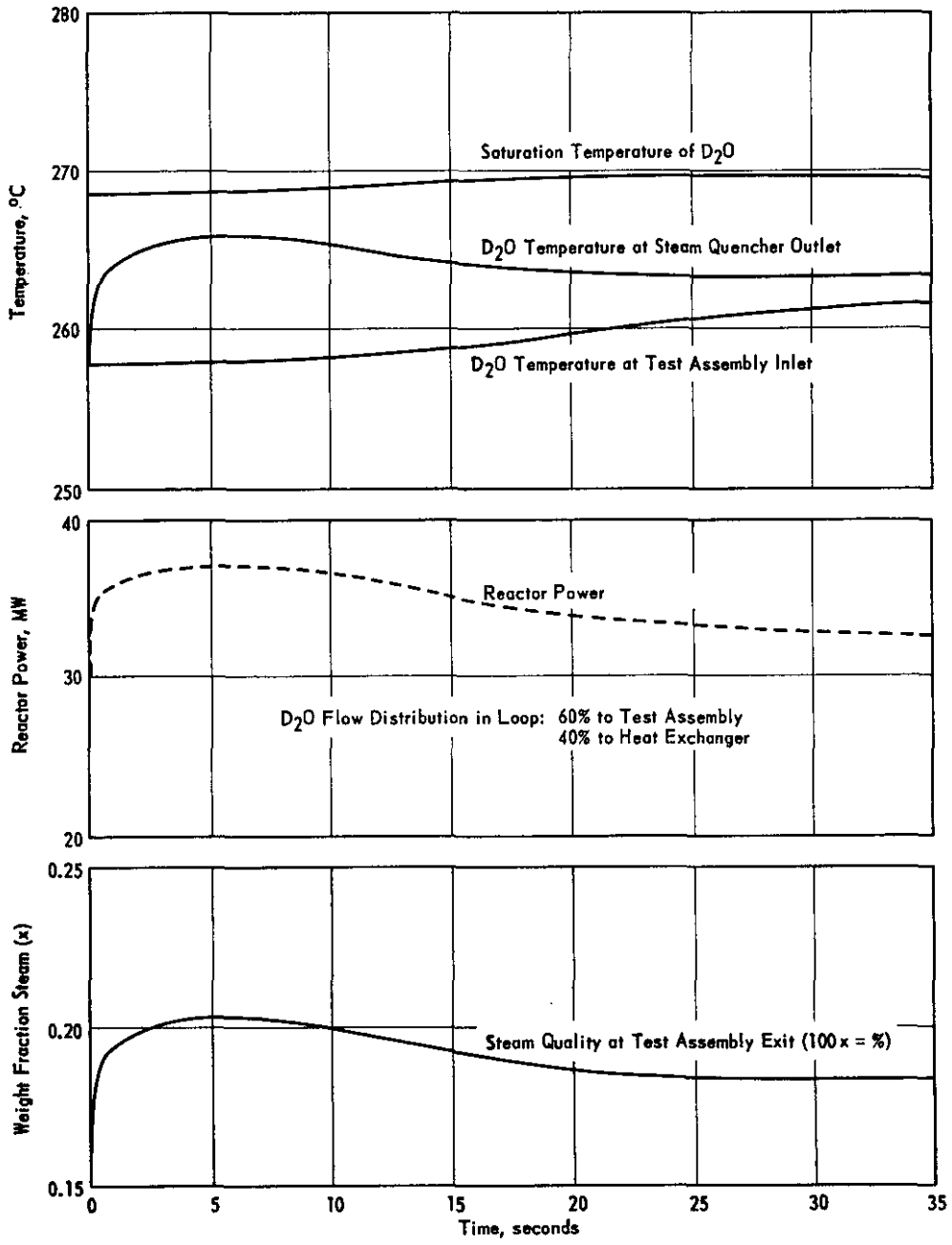

FIG. 6 TRANSIENT RESPONSE OF BOILING LOOP OF HWCTR TO STEP INCREASE OF 0.001 k IN REACTIVITY

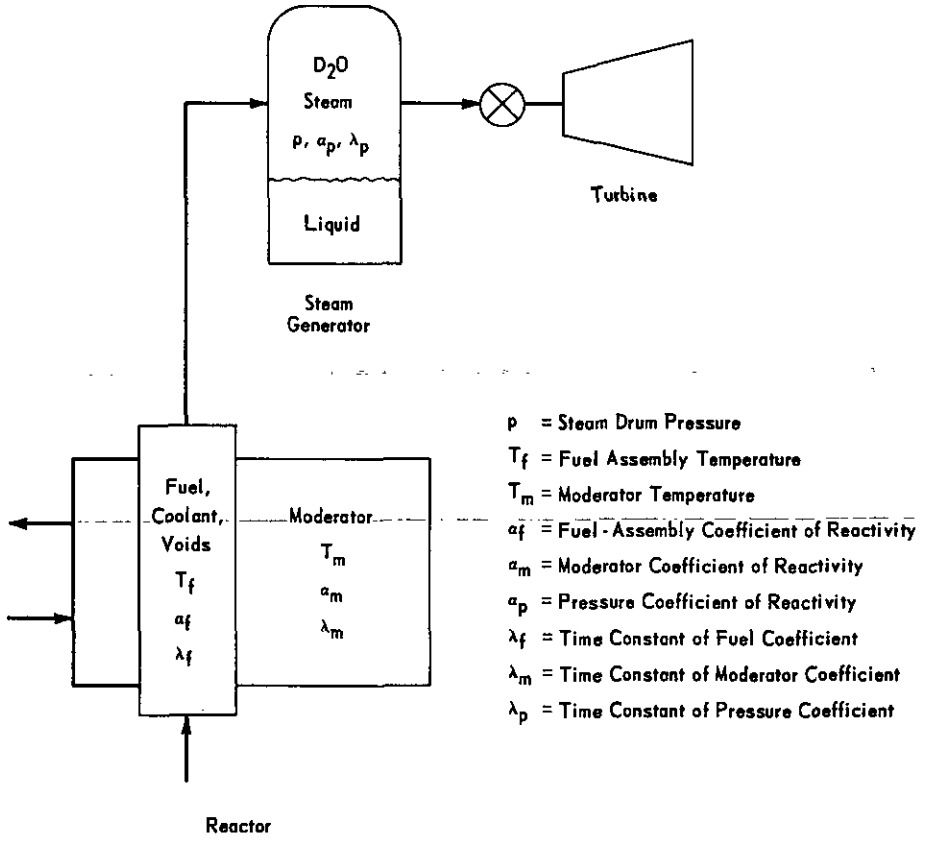

FIG. 7 SIMPLIFIED REPRESENTATION OF THE BOILING REACTOR SYSTEM

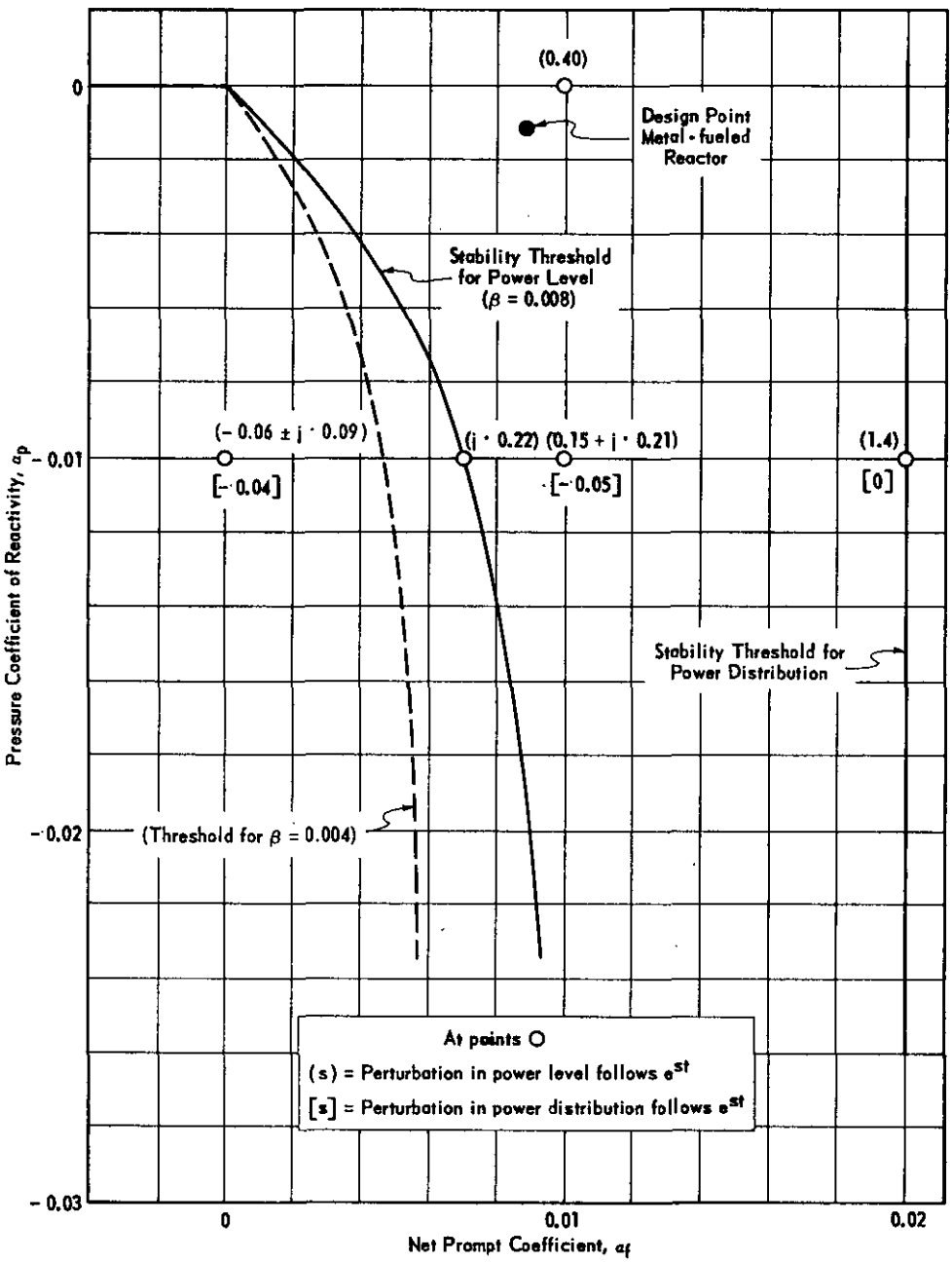

FIG. 8 STABILITY REGIONS FOR A BOILING REACTOR

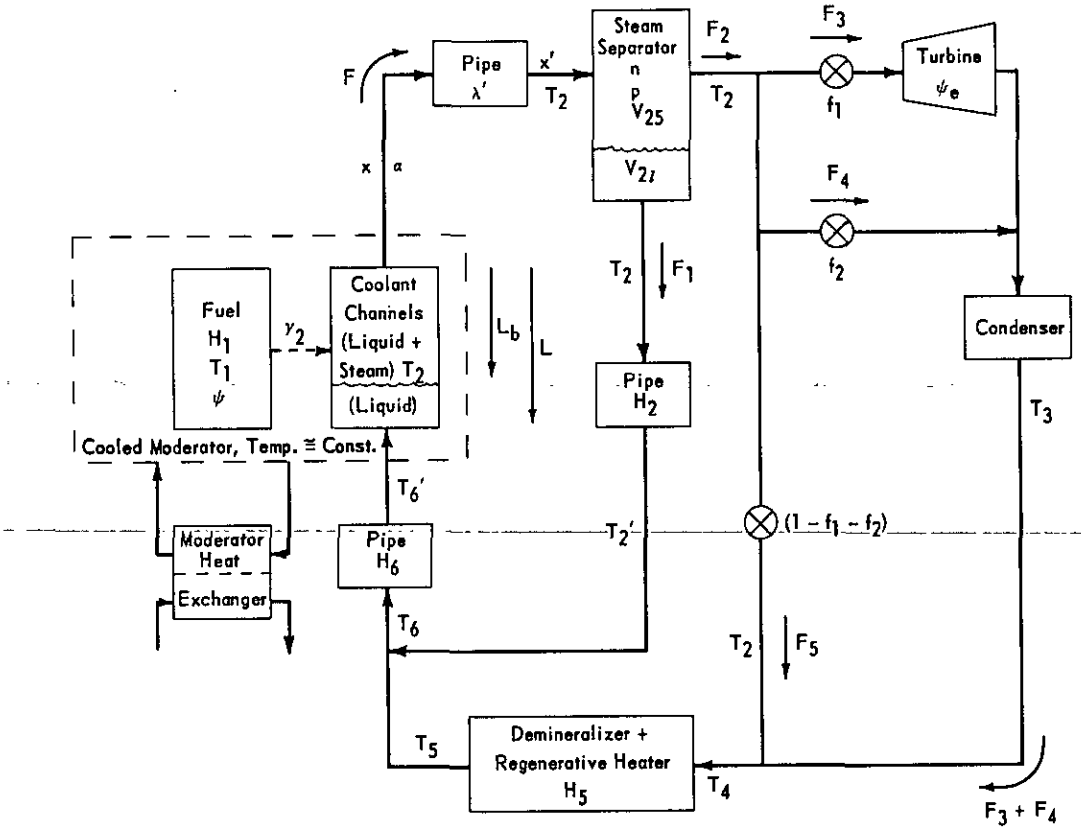

FIG. 9 BLOCK DIAGRAM OF BOILING POWER REACTOR

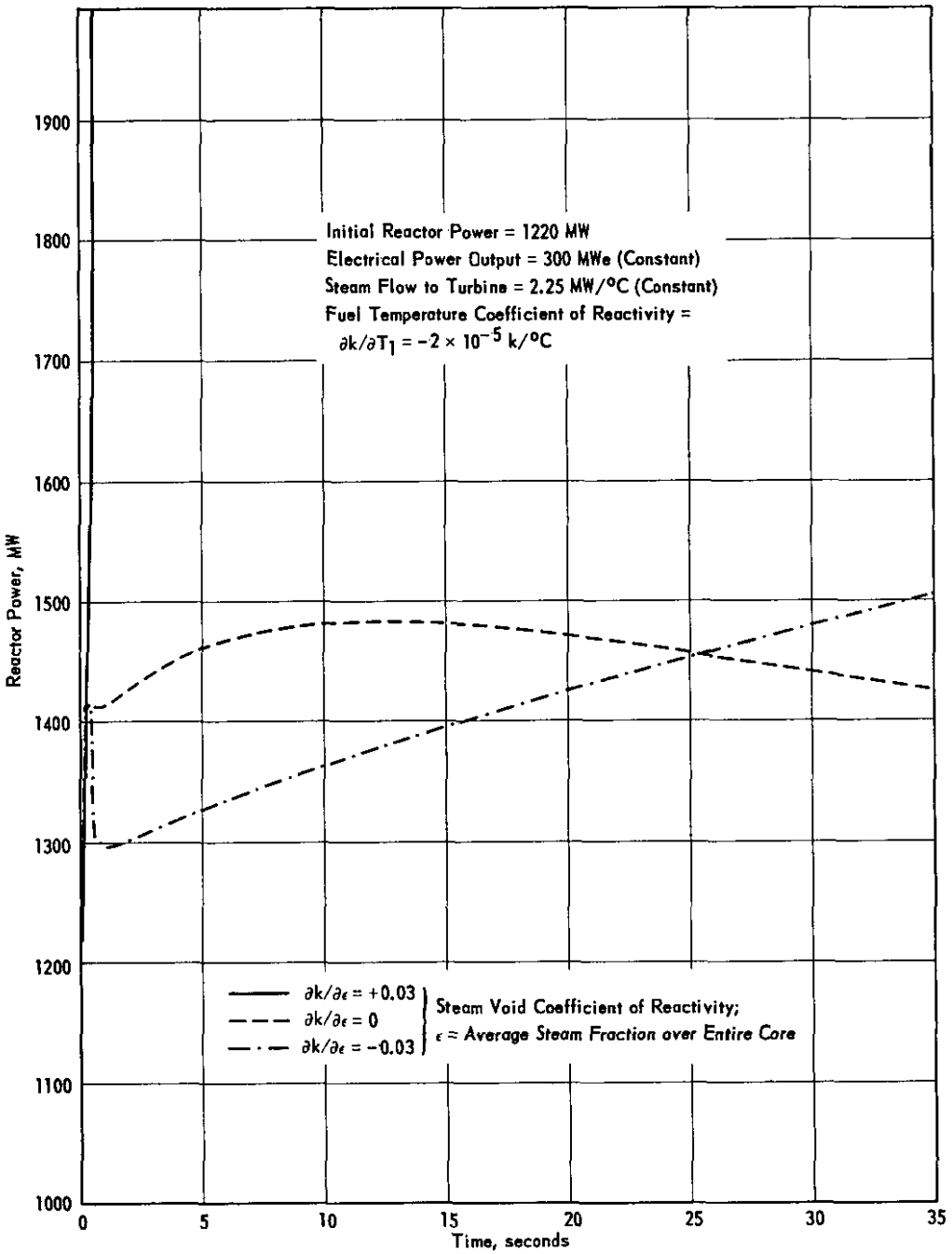

FIG. 10 RESPONSE OF METAL-FUELED BOILING D_2O REACTOR TO STEP INCREASE IN REACTIVITY OF 0.001 k

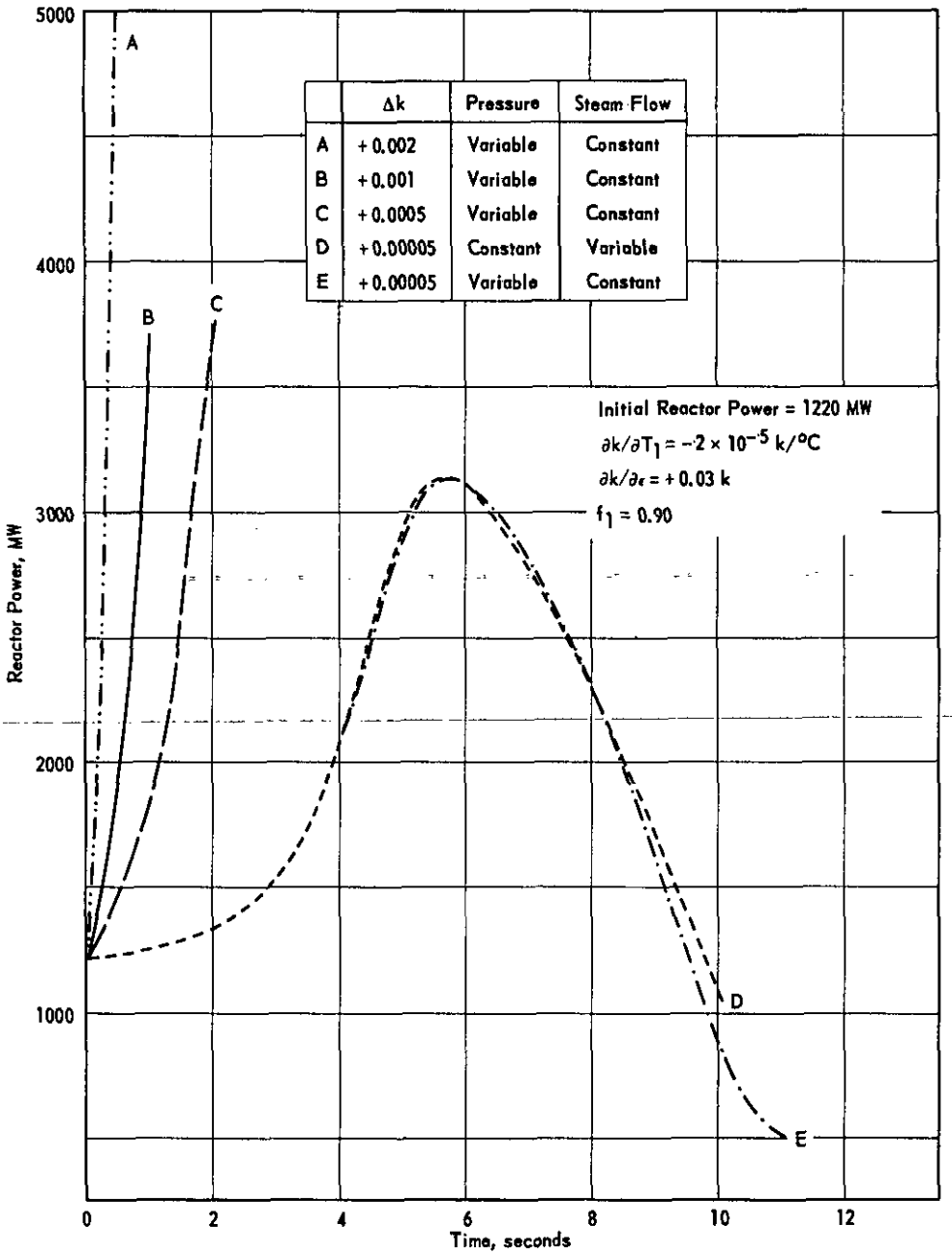

FIG. 11 RESPONSE OF METAL-FUELED BOILING D_2O REACTOR TO VARIOUS STEP INCREASES IN REACTIVITY

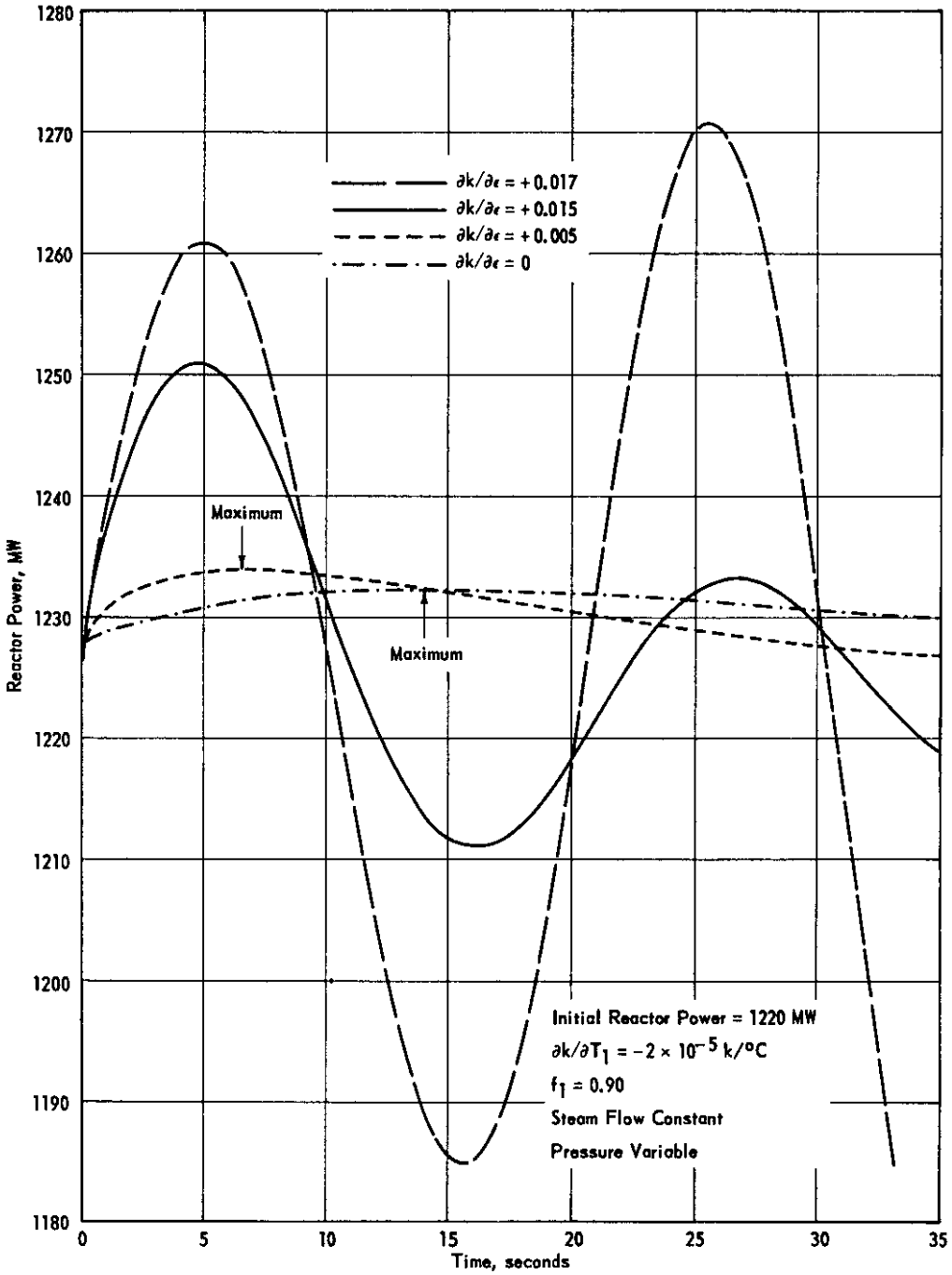

FIG. 12 RESPONSE OF METAL-FUELED BOILING D_2O REACTOR TO STEP INCREASE IN REACTIVITY OF 0.00005 k

Void Coefficients near Threshold of Instability

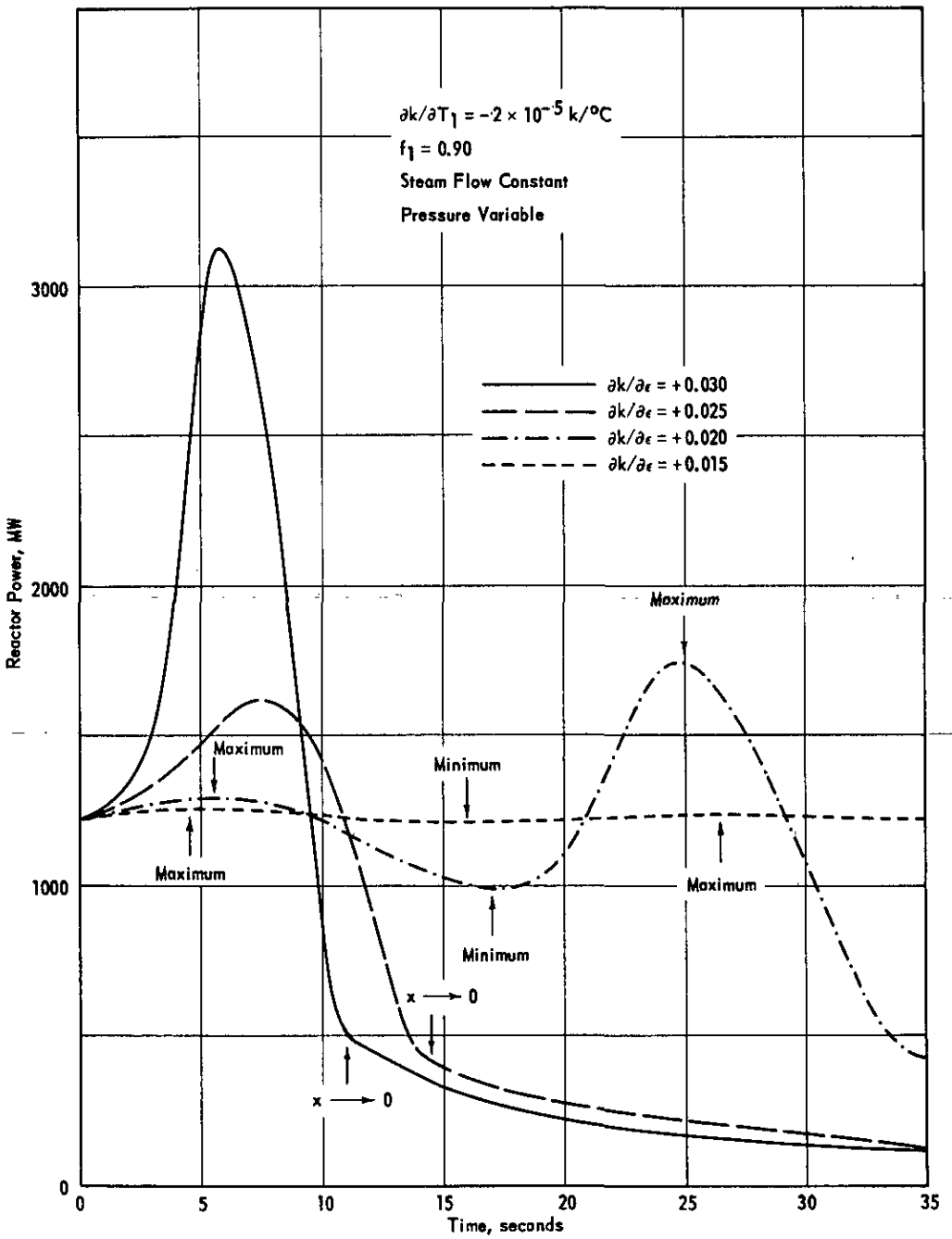

FIG. 13 RESPONSE OF METAL-FUELED BOILING D_2O REACTOR TO STEP INCREASE IN REACTIVITY OF 0.00005 k

Void Coefficients Beyond Threshold of Instability

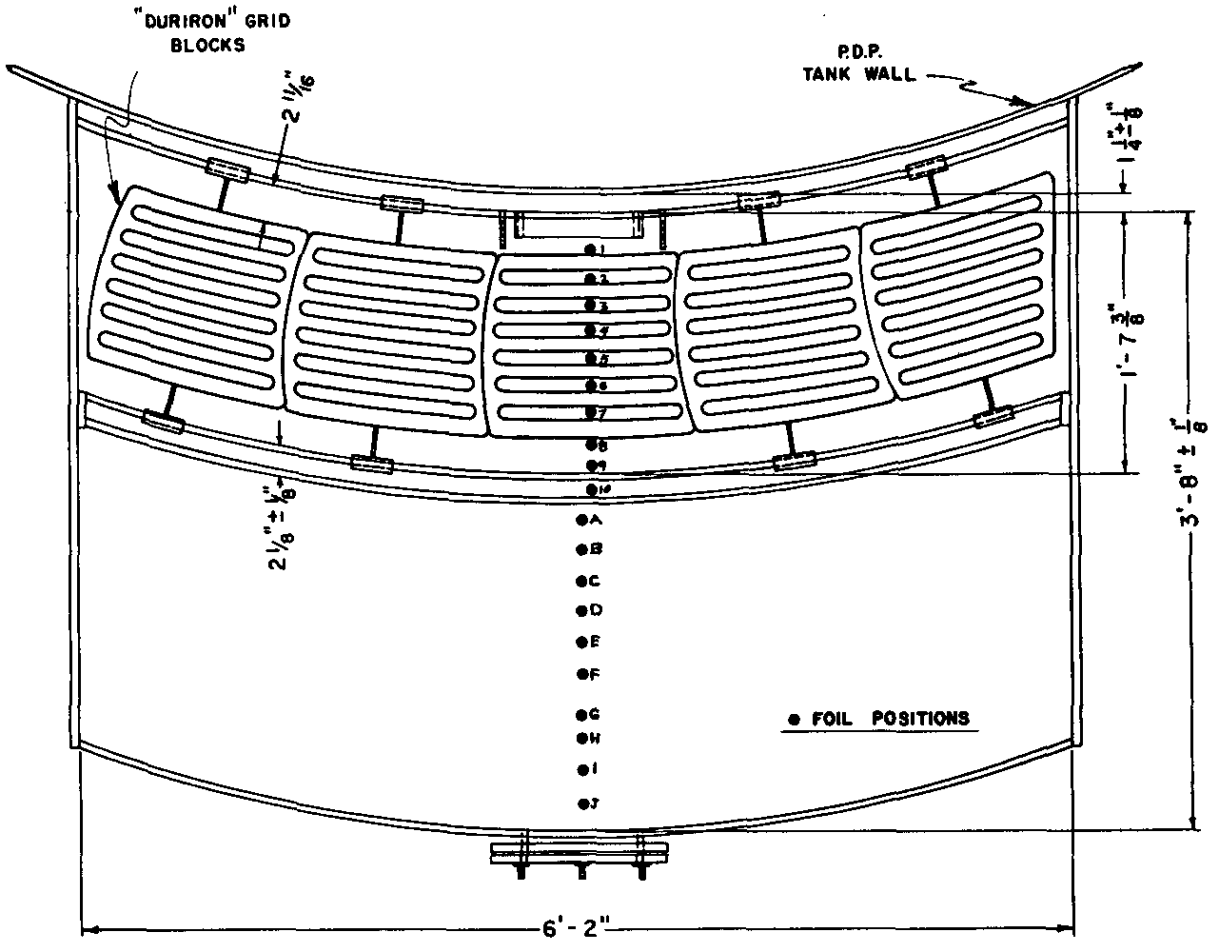

FIG. 14 TOP VIEW OF PDP SHIELD TANK WITH FOIL POSITIONS INDICATED

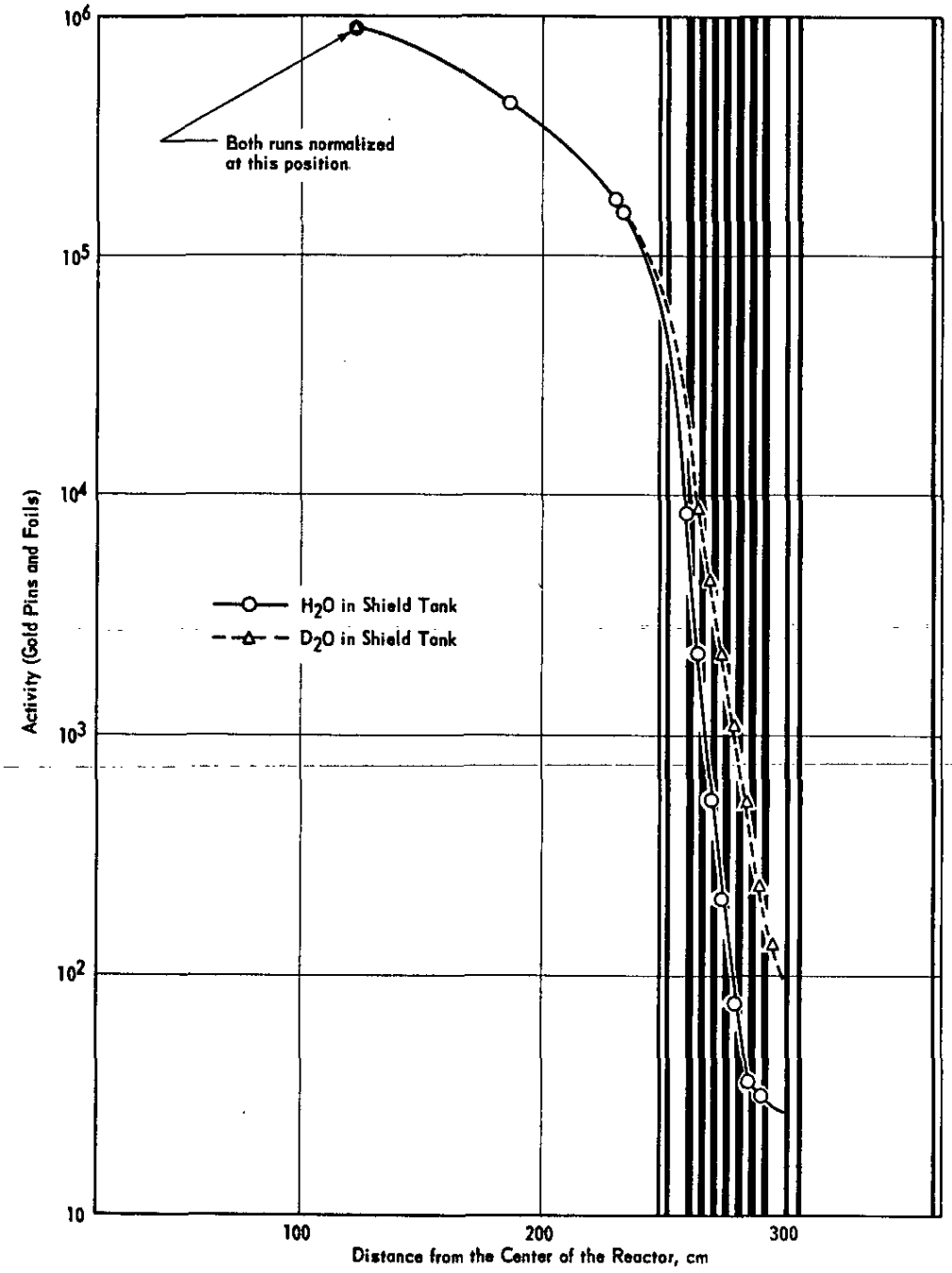

FIG. 15 ACTIVITY vs. R FOR GOLD PINS AND FOILS IN THE PDP AND THE SHIELD TANK

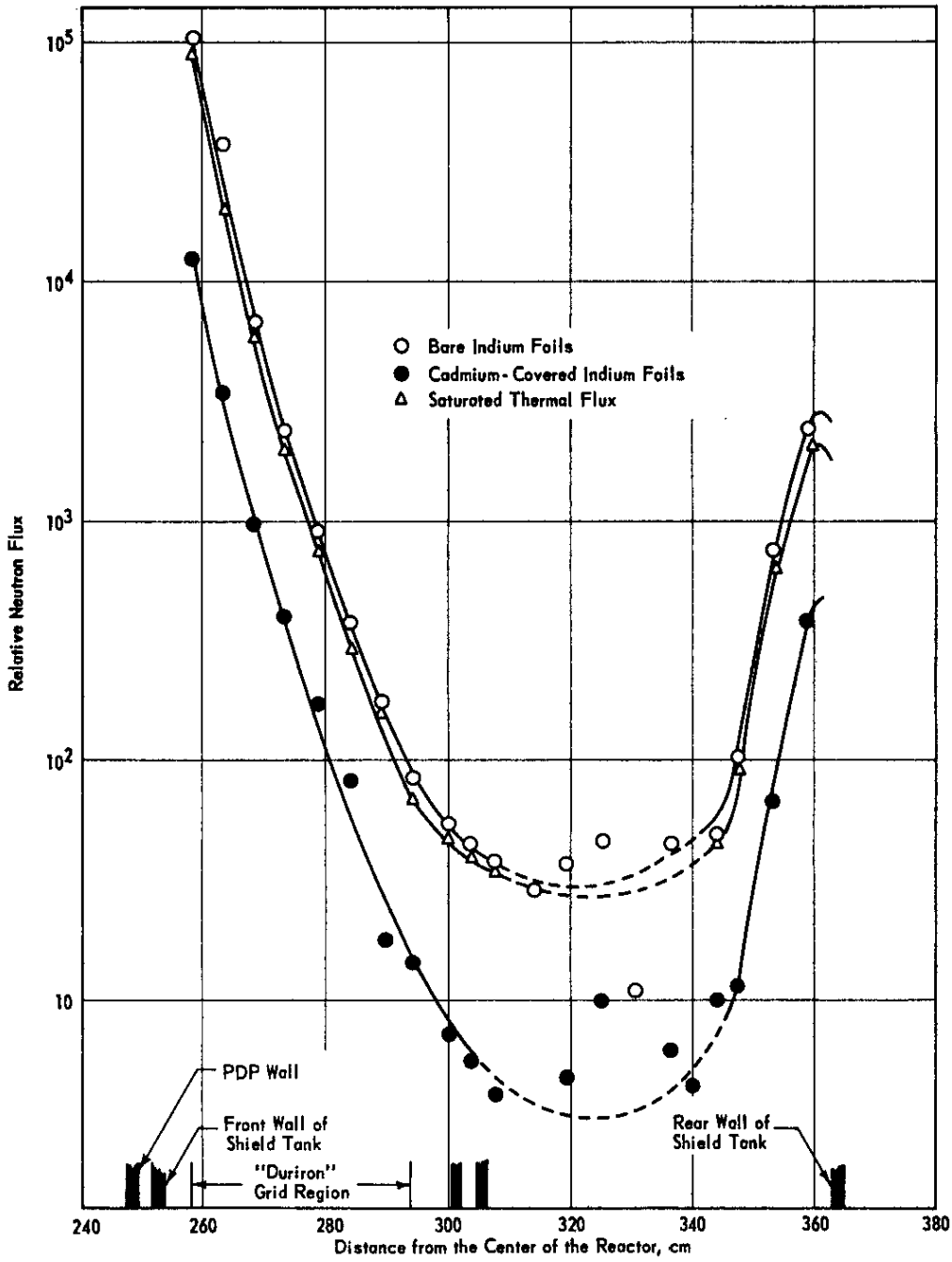

FIG. 16 RELATIVE NEUTRON FLUX THROUGH THE PDP SHIELD MOCKUP WHEN FILLED WITH H_2O

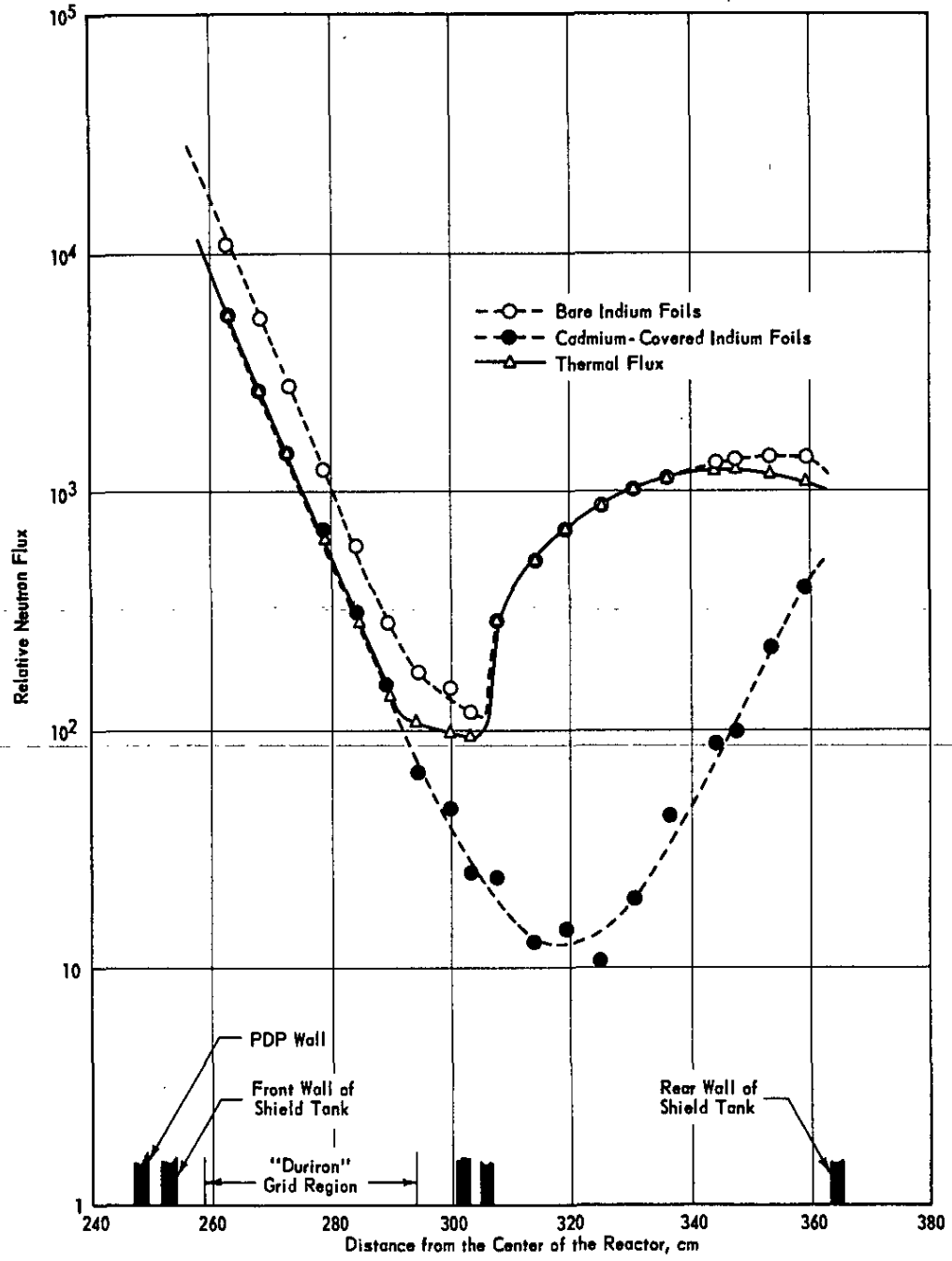

FIG. 17 RELATIVE NEUTRON FLUX THROUGH THE PDP SHIELD MOCKUP WHEN FILLED WITH D_2O

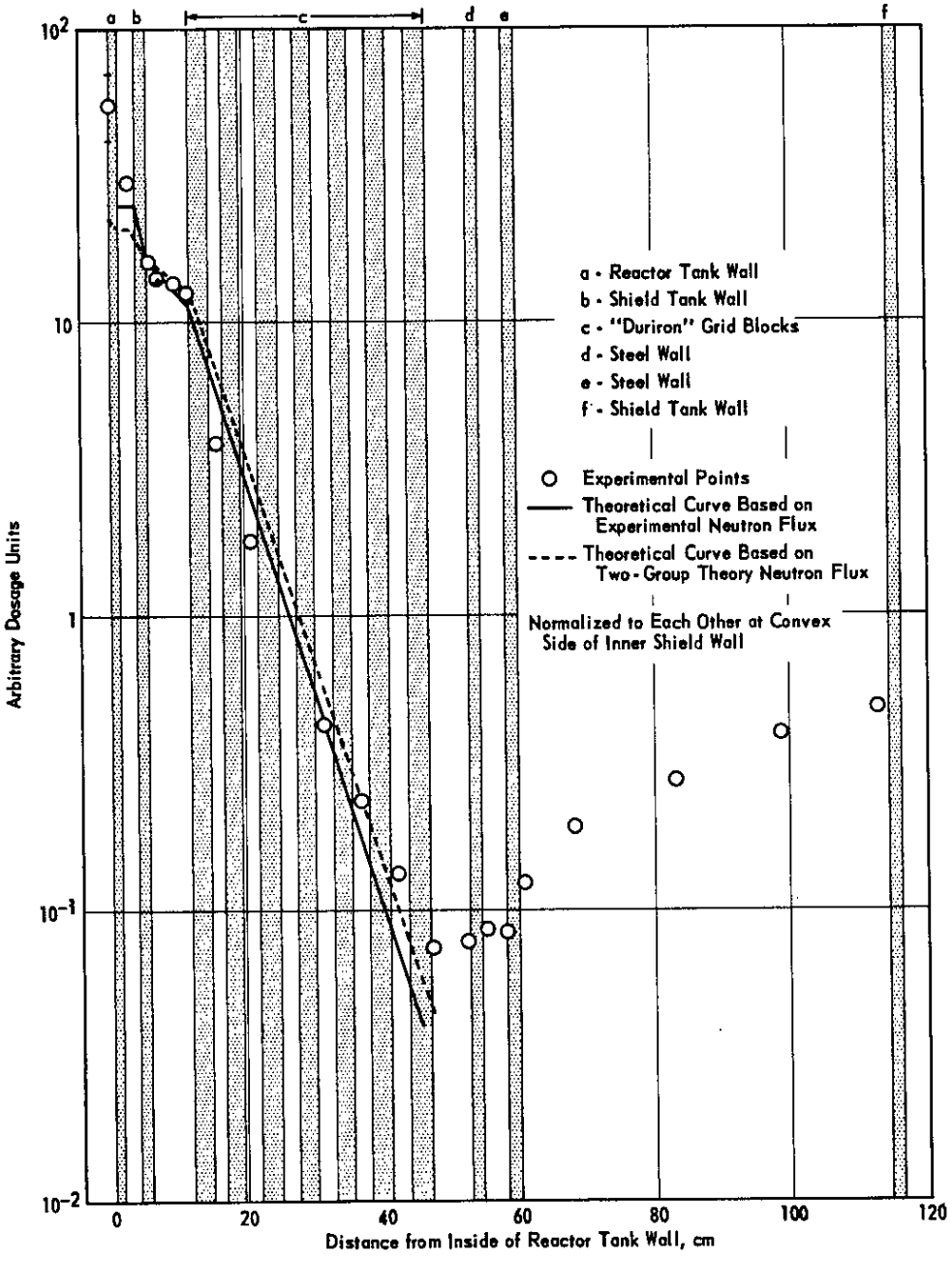

FIG. 18 COMPARISON OF EXPERIMENTAL AND THEORETICAL GAMMA DISTRIBUTIONS THROUGH SHIELD TANK

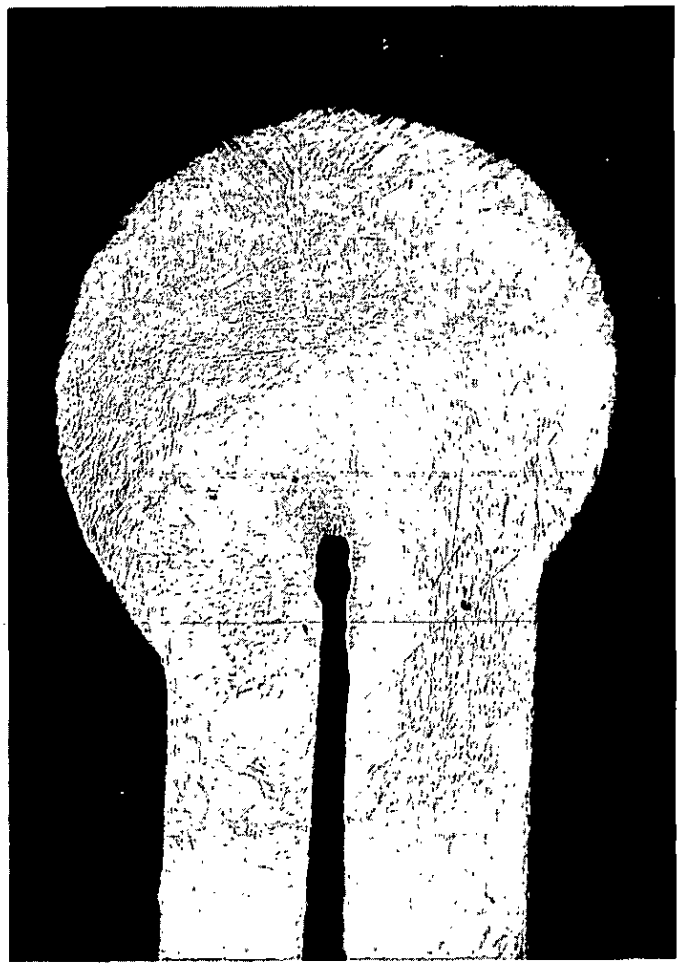

50X

Outer Weld, As Polished

FIG. 19 CROSS SECTION OF ELECTRON-BEAM WELD BETWEEN SHEATH AND END PLUG OF Zr-CLAD URANIUM TUBE

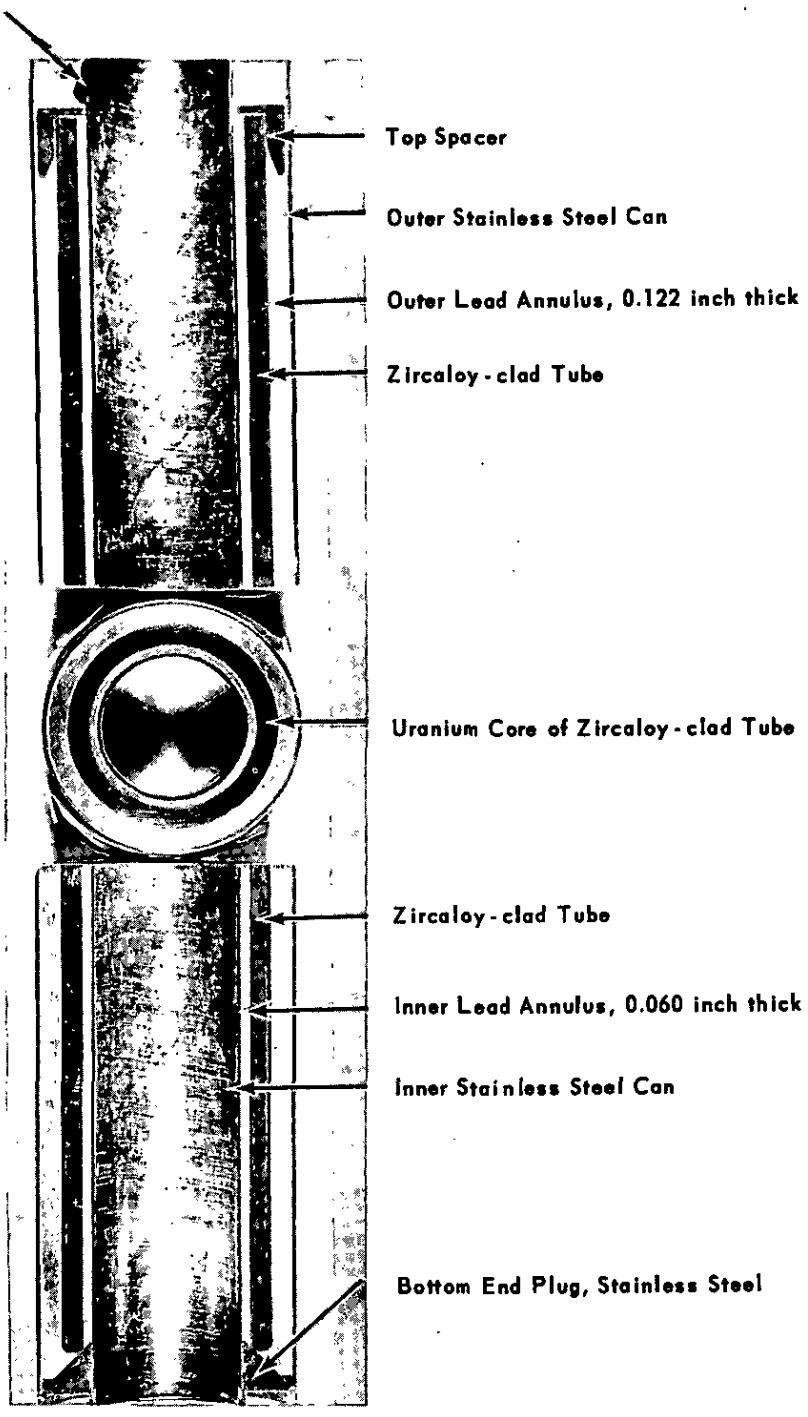

FIG. 20 LEAD-INSULATED CAPSULE FOR HIGH-TEMPERATURE IRRADIATION TESTING OF Zr-CLAD URANIUM TUBES

0.7X

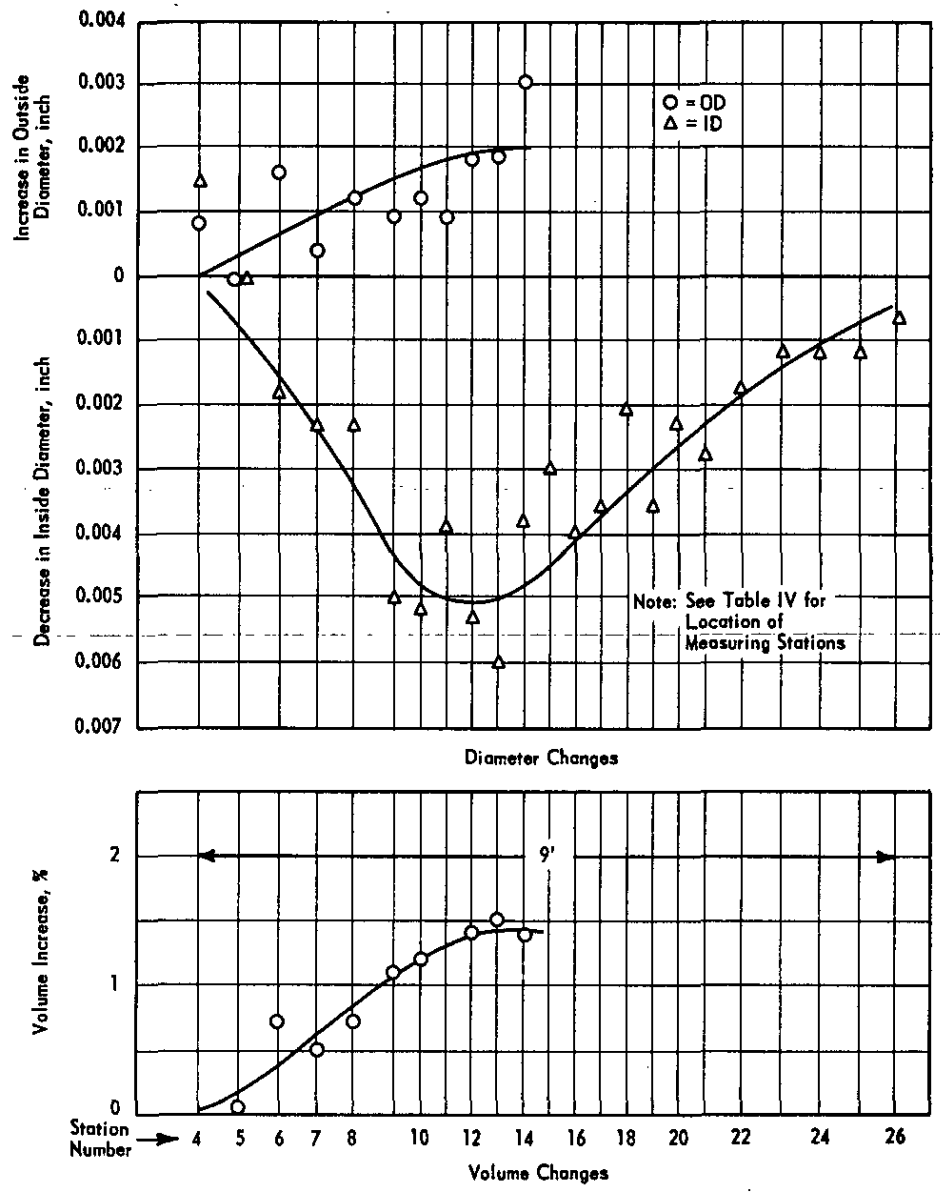

FIG. 21 GROWTH OF UNALLOYED URANIUM TUBE DURING IRRADIATION IN THE NRU REACTOR

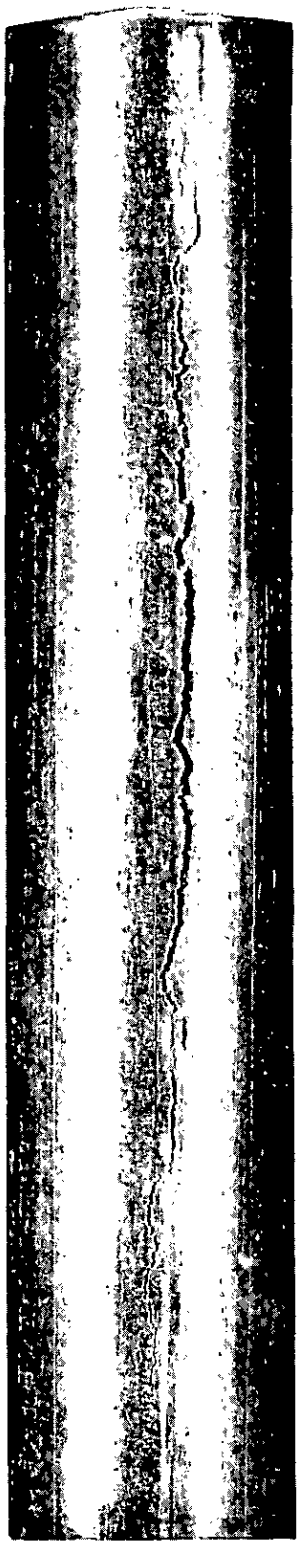

FIG. 22 SHEATH FAILURE IN A UO_2 FUEL TUBE
(Swaged Stainless Steel Sheath)

0.7X

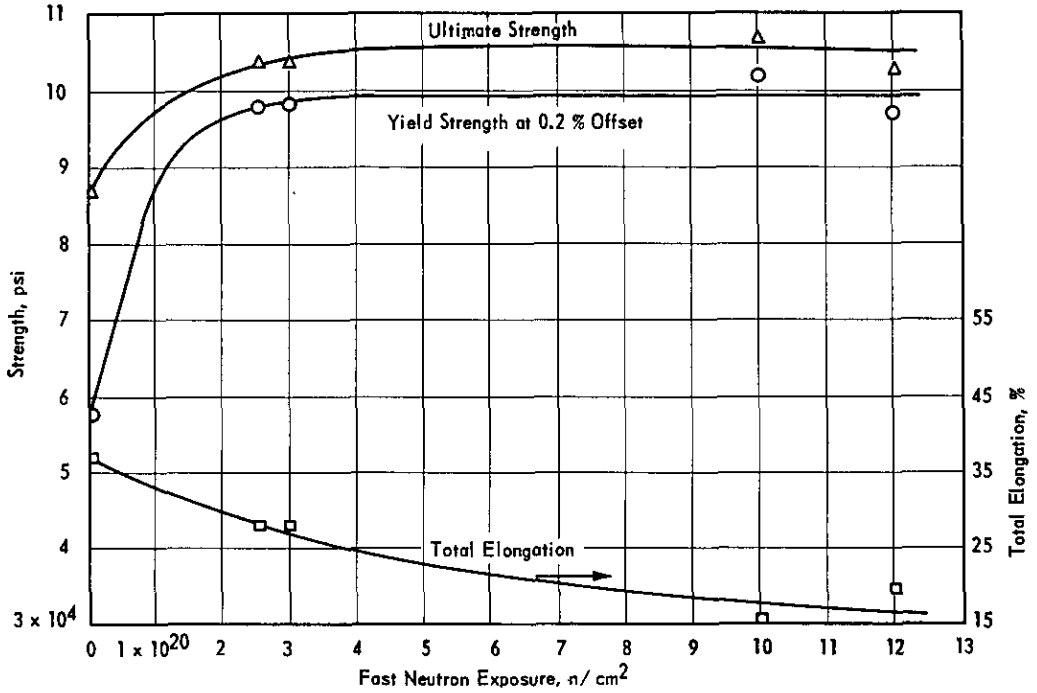

FIG. 23 EFFECT OF IRRADIATION ON TENSILE PROPERTIES OF STAINLESS STEEL WELD METAL

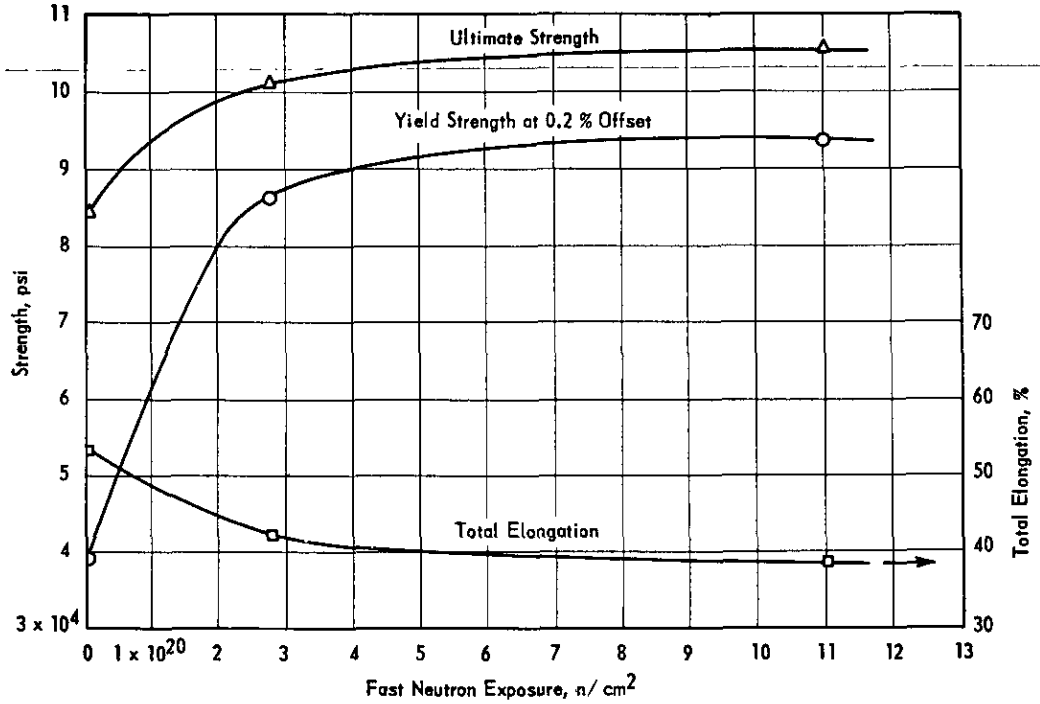

FIG. 24 EFFECT OF IRRADIATION ON TENSILE PROPERTIES OF STAINLESS STEEL HEAT-AFFECTED ZONE

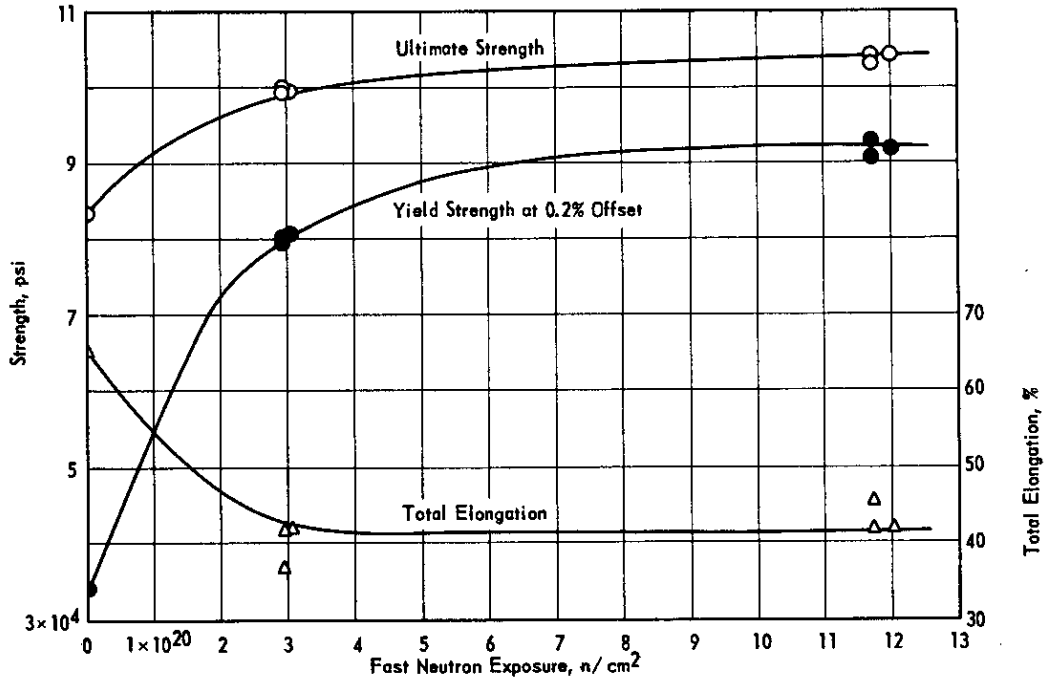

FIG. 25 EFFECT OF IRRADIATION ON TENSILE PROPERTIES OF STAINLESS STEEL PARENT PLATE

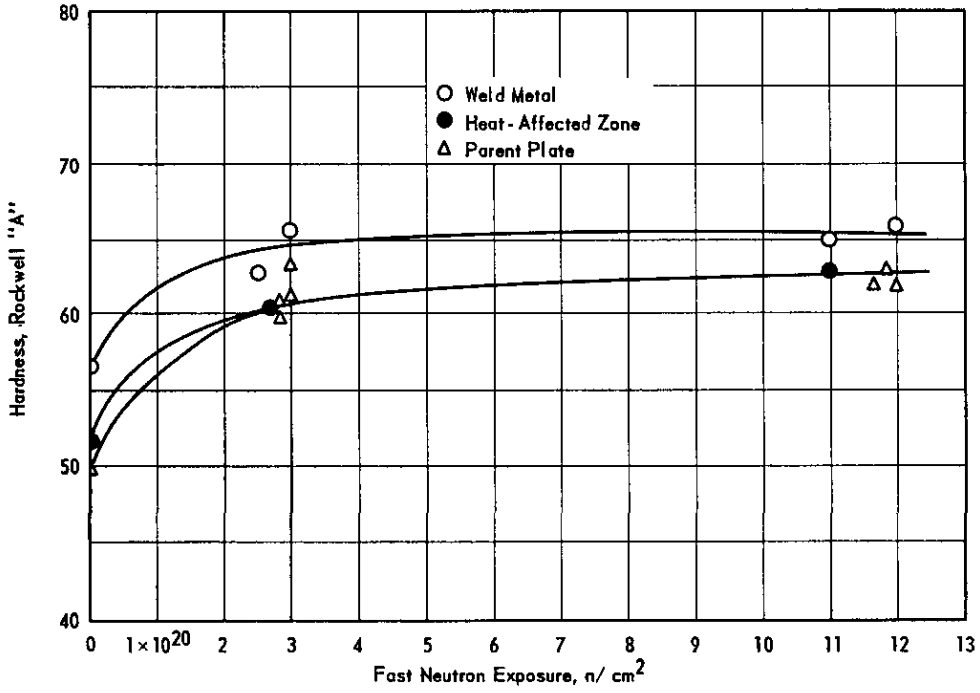

FIG. 26 EFFECT OF IRRADIATION ON HARDNESS IN STAINLESS STEEL WELDS

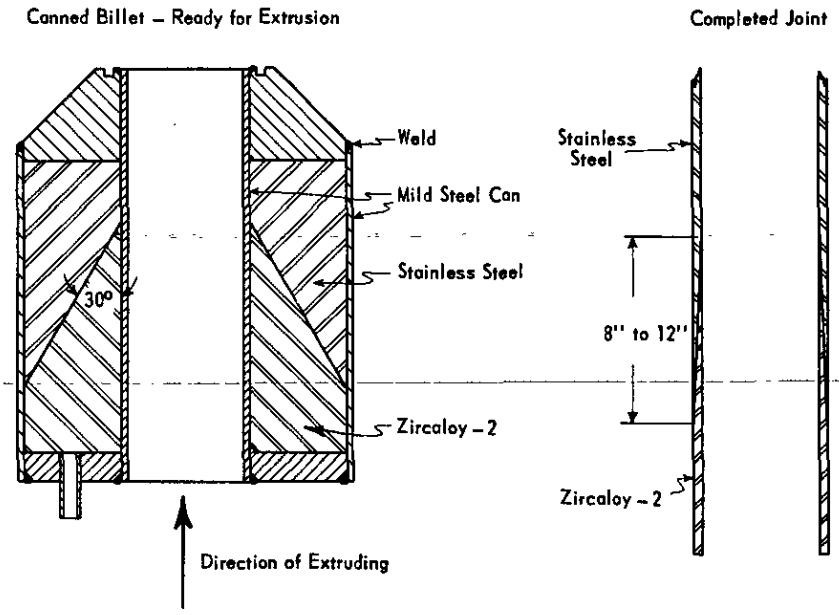

FIG. 27 TANDEM-EXTRUDED JOINT OF ZIRCALOY AND STAINLESS STEEL

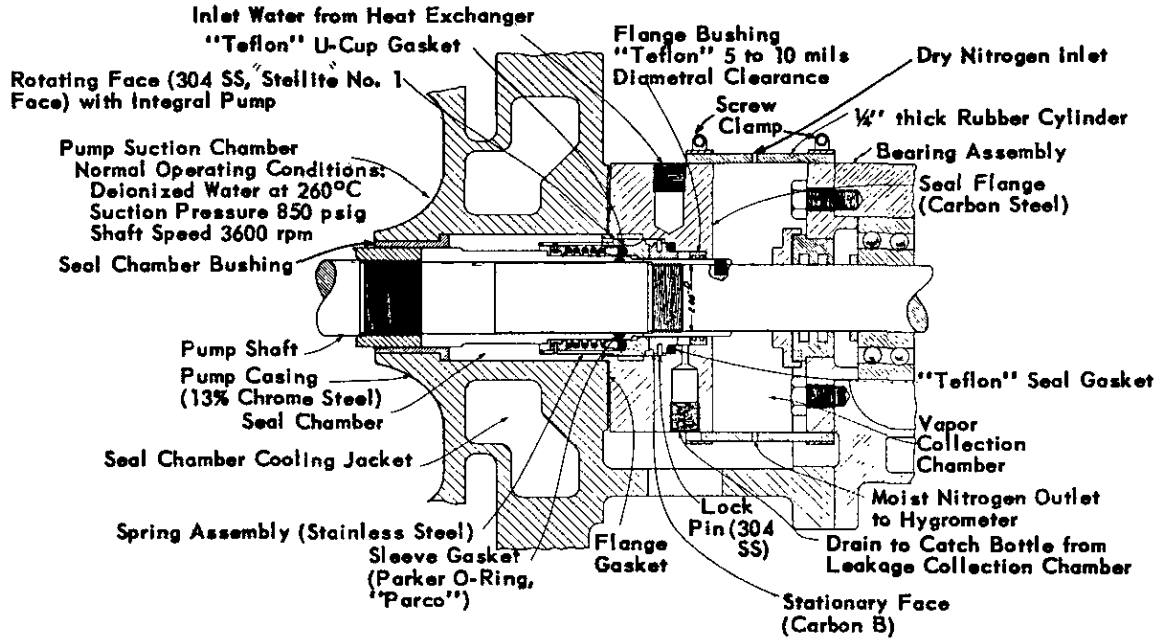

Assembly of Outboard Mechanical Seal
B.J. D-2250 Mechanical Seal
Pacific 8 x 10½ HVC

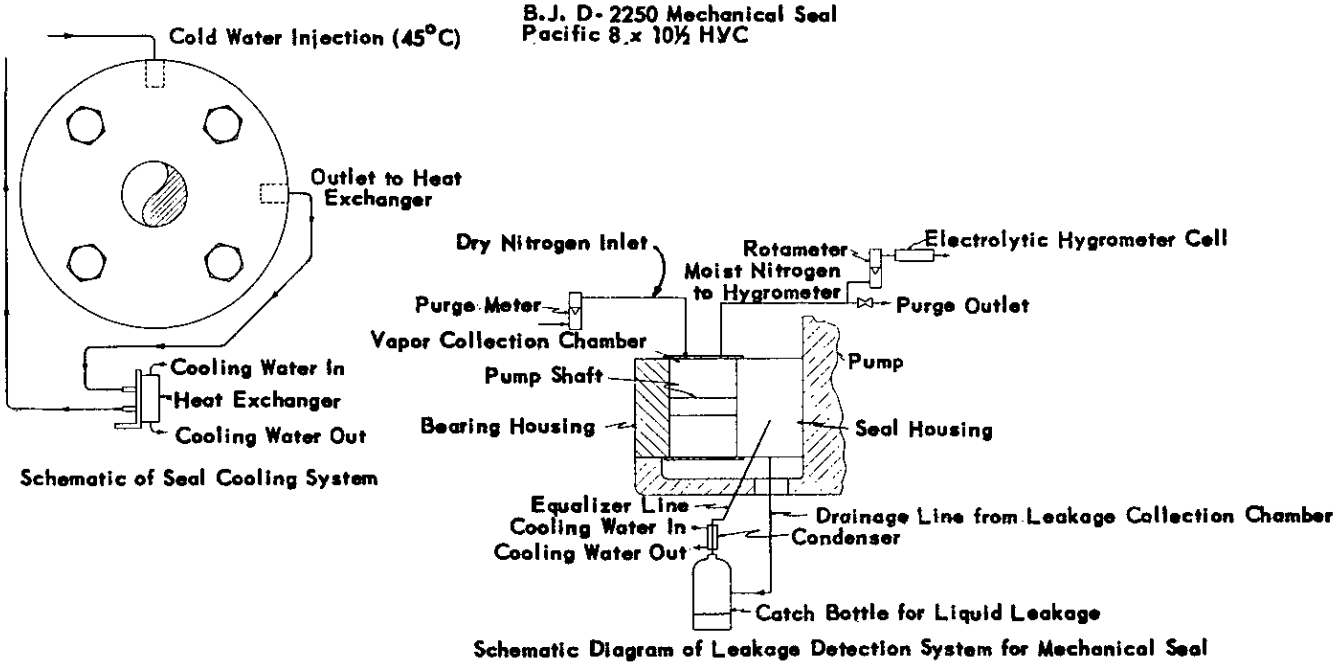

Schematic of Seal Cooling System

Schematic Diagram of Leakage Detection System for Mechanical Seal

FIG. 28 EQUIPMENT ARRANGEMENT FOR DETECTION OF WATER LEAKAGE FROM MECHANICAL SEALS